environments

MDPI

Article

An Integrated Geospatial Framework for Urban Vulnerability Assessment and Adaptation Prioritization Under Environmental and Flood-Related Stressors

Detchphol Chitwatkulsiri [1,*], Ratchaphon Charoenpanuchart [1], Adichai Pornprommin [1] and Kim Neil Irvine [2]

[1] Department of Water Resources Engineering, Faculty of Engineering, Kasetsart University, Bangkok 10900, Thailand; ratchaphon.cha@ku.th (R.C.); fengacp@ku.ac.th (A.P.)
[2] Thammasat University Research Unit for Nature-Based Solutions in Water Management, Faculty of Architecture and Planning, Thammasat University Rangsit Campus, Khlong Luang, Pathum Thani 12121, Thailand; kim.irvine@ap.tu.ac.th
* Correspondence: detchphol.ch@ku.th

Abstract

Urban flooding is an increasingly complex challenge in highly urbanized environments, where environmental stress, infrastructure limitations, and flood-related pressures influence community vulnerability. Conventional flood assessments provide valuable hazard information but often overlook environmental conditions. Furthermore, the use of crowd-sourced inundation reports to validate flood modelling approaches, particularly in data-scarce areas, often is overlooked. While vulnerability indices consider environmental, social, and economic factors, this study focuses on developing an integrated geospatial framework to assess and prioritize urban vulnerability by combining UHI-related environmental stress, drainage density, and flood depth derived from hydraulic modeling and supported by social media observations. The framework was tested on the Ratchadaphisek–Phahonyothin–Kasetsart Intersection Polder in Bangkok, Thailand. UHI-related environmental stress characterized urban conditions, drainage density represented the availability of drainage infrastructure, and social media observations supported flood extent identification and model validation. These datasets were integrated to develop an Urban Vulnerability Index (UVI) and identify spatial concentrations of vulnerability. The results showed substantial spatial variability, with approximately 61.9% of the study area classified as having Moderate to Very High vulnerability. Areas with elevated environmental stress, limited drainage infrastructure, and greater flood depth exhibited higher vulnerability. Spatial prioritization identified Kamphaeng Phet 1 and 4 Roads, Ratchadaphisek Road, and Lat Phrao Intersection as the highest-priority intervention locations. Building-level assessment classified 30,394 buildings (39.4% of the total) within the High and Very High vulnerability categories. Integrating earth observation, drainage infrastructure, hydraulic modeling, and citizen-generated observations provides a broader understanding of urban vulnerability and supports spatial prioritization, adaptation planning, infrastructure investment, and urban resilience strategies. Future research could consider additional geospatially explicit indicators, including air quality, noise, green-space quality and extent, transportation patterns, and demographic characteristics such as income status.

Keywords: urban vulnerability index; urban heat island; flood adaptation; social media; GIS

Academic Editor: Chin H. Wu

Received: 7 October 2026
Revised: 5 November 2026
Accepted: 23 November 2026
Published: 26 November 2026

Copyright: © 2026 by the authors. Licensee MDPI, Basel, Switzerland. This article is an open access article distributed under the terms and conditions of the Creative Commons Attribution (CC BY) license.

1. Introduction

Flood management is a challenging issue in densely developed urban environments, where environmental conditions, infrastructure performance, and human exposure collectively influence flood impacts [1,2]. Although conventional flood assessment has advanced through hydrological modeling, remote sensing, and terrain-based analysis, existing approaches predominantly emphasize physical flood processes and often provide limited understanding of how urban built and social characteristics contribute to vulnerability and observed impacts [3–7].

Among the environmental processes shaping urban conditions, the Urban Heat Island (UHI) effect has received increasing attention due to its association with urban expansion and surface modification [8,9]. Elevated urban temperatures are commonly linked to extensive impervious surface space, reduced vegetation cover, and altered surface energy exchange, and have been widely characterized using satellite-derived thermal observations [10–13]. Beyond thermal conditions, UHI has increasingly been recognized as an indicator of accumulated environmental stress and broader urban surface characteristics [14–16]. UHI can increase localized rainfall intensity, although climate change and increasing global temperatures may complicate this relationship [17,18]. UHI also has complex relationships with air quality, including fine particulate matter (PM2.5) and other pollutants, as well as with urban design characteristics such as building materials, blue-green space and transport, and human health [19–21]. In parallel, drainage systems play an essential role in regulating stormwater conveyance and reducing flood accumulation. Variations in drainage density may influence local drainage efficiency and contribute to differences in flood sensitivity across urban areas [22–25].

Recent advances in digital technologies have introduced social media as a complementary source of environmental observations [26–28]. Citizens increasingly have documented flood conditions through geolocated posts, photographs, and real-time reports, providing direct evidence of impacts experienced during flood events [29,30]. Previous studies have demonstrated the usefulness of these observations for disaster monitoring and flood assessment, particularly in enhancing spatial coverage and capturing localized impacts that may not be represented by conventional monitoring systems [31,32]. We do recognize the potential spatial bias that may be incurred by social media approaches [33,34], but in data-scarce environments crowd-sourced information may enhance information on flood vulnerability that is not available from traditional official monitoring [35].

In flood modelling specifically, citizen and social media observations have mostly been used to check simulated inundation qualitatively, for example by overlaying geotagged reports on modelled flood maps, or to reconstruct flood conditions at individual reported points [29,36]. Quantitative comparisons between such observations and model outputs remain uncommon because the data are typically presence-only (they record where flooding was reported but not where it was absent), unevenly distributed in space, and limited in number, which restricts the use of standard contingency-based skill scores [36]. In addition, these observations have rarely been used beyond model evaluation, for example, to examine where reported and simulated flooding coincides with other urban stressors. The present study addresses this second gap: social media observations are used as independent spatial evidence for evaluating a calibrated two-dimensional hydraulic model; the simulated flood depth is then combined with environmental stress and drainage indicators in a single vulnerability assessment.

Despite growing interest in thermal environments, drainage characteristics, and citizen-generated observations, these information sources remain largely investigated independent of each other [14]. Existing studies commonly focus on environmental characterization, drainage performance, or flood occurrence separately, resulting in limited understanding of how environmental stress, infrastructure conditions, and observed impacts

https://doi.org/10.3390/environments13120653

interact spatially to shape urban vulnerability [1,2,37–40]. This is, however, starting to change through ecosystem service assessments that consider several urban functions together [41]. From a resilience perspective, vulnerability emerges through the interaction between environmental pressure, adaptive infrastructure capacity, experienced impacts, and socioeconomic factors such as income, preparedness, and access to resources [42–44]. In this study, urban vulnerability refers to the combination of physical flooding and environmental stresses as represented by the UHI. Areas exhibiting elevated environmental stress, inadequate drainage infrastructure, and greater flood exposure are considered to possess higher levels of vulnerability. This conceptualization is consistent with vulnerability frameworks that emphasize the interaction between environmental conditions, system capacity, and hazard-related impacts in shaping spatial patterns of risk and resilience [45]. Vulnerability is also shaped by socioeconomic conditions and by the cultural ecosystem services provided by urban green and blue spaces [41]; these dimensions are not represented in the present index and are identified as directions for future work (Section 5).

Within the widely used risk framework that distinguishes hazard, exposure, sensitivity and adaptive capacity [45], the three components of the proposed index play different roles. Flood depth represents the flood hazard and exposure of the urban area to inundation. Drainage density represents the availability of drainage infrastructure and is used as a proxy for the physical coping capacity of the urban drainage system. Other water-related stresses in Bangkok include (i) long-term groundwater abstraction from the multi-layered Bangkok aquifer system, which has caused land subsidence that increases flood exposure, with hydrogeochemical and isotopic studies documenting groundwater salinization within this aquifer system [46,47]; (ii) urban water quality issues associated with flooding [48]; and (iii) mortality and wellbeing stress associated with floods [49–53]. These hydrologic and hydro-geochemical dimensions are important components of environmental stress in Bangkok; however, assessing them requires water quality sampling, subsurface data, and community wellbeing surveys that were not available at the 100 × 100 m resolution adopted in this study. The present framework therefore focuses on the surface-related dimension of environmental stress that can be mapped consistently across the study area and these other environmental and wellbeing dimensions are identified as a direction for future extension of the framework. UHI-related environmental stress represents the physical sensitivity of the urban surface: the impervious, densely built, and poorly vegetated conditions that raise surface temperatures also increase runoff generation and reduce infiltration. This component therefore does not imply that higher temperatures themselves make an area more susceptible to flooding; rather, it is an indicator that represents a combination of thermal comfort and health/wellbeing stress associated with urban typologies and anthropogenic activities. Socioeconomic sensitivity, the capacity of households and communities to prepare for and recover from floods, and the characteristics of the exposed population have not been included at this point in our research program for the site. The index should therefore be interpreted as a measure of physical flood and representative aspects of urban environmental wellbeing vulnerability rather than a direct measure of social or community vulnerability, which would require additional socioeconomic and demographic indicators.

A specific limitation of considering the UHI-related environmental stress, drainage density, and flood depth indicators independently is that spatially-explicit information on where the stressors overlap is not considered, for example, where intensive urban surface conditions coincide with sparse drainage infrastructure and simulated inundation. Conventional flood hazard maps rank locations by inundation alone and single-factor indices rank them by one stressor at a time; neither distinguishes an area exposed to one stressor from an area where several stressors compound. Without a spatial overlay of these

stressors at a common resolution, adaptation resources may be poorly targeted. This multi-stressor overlay is the gap that the present framework is designed to fill.

Accordingly, this study develops an integrated GIS-based framework by combining satellite-derived UHI-related environmental stress, drainage density, and flood-related information derived from hydraulic modeling and supported by social media observations [54–58]. These datasets were spatially integrated to construct an Urban Vulnerability Index (UVI) and identify areas where environmental stress, drainage constraints, and Flood-Related Information converge. The proposed framework provides a spatial prioritization approach to support climate adaptation and urban resilience planning [42,58,59].

2. Materials and Methods

2.1. Research Framework

This study adopts an integrated geospatial framework to assess and prioritize urban vulnerability under environmental and flood-related stressors (Figure 1). The framework consists of four analytical stages.

First, environmental, infrastructure, and flood-related datasets were collected from multiple sources. Second, these datasets were processed to generate spatial layers representing environmental stress, drainage density, and flood depth. Third, the resulting layers were integrated to develop an Urban Vulnerability Index (UVI) and identify vulnerable urban areas. Finally, vulnerability-related outputs, including vulnerability maps, hotspot zones, building-level assessments, and priority ranking areas, were generated to support flood adaptation planning and urban resilience strategies.

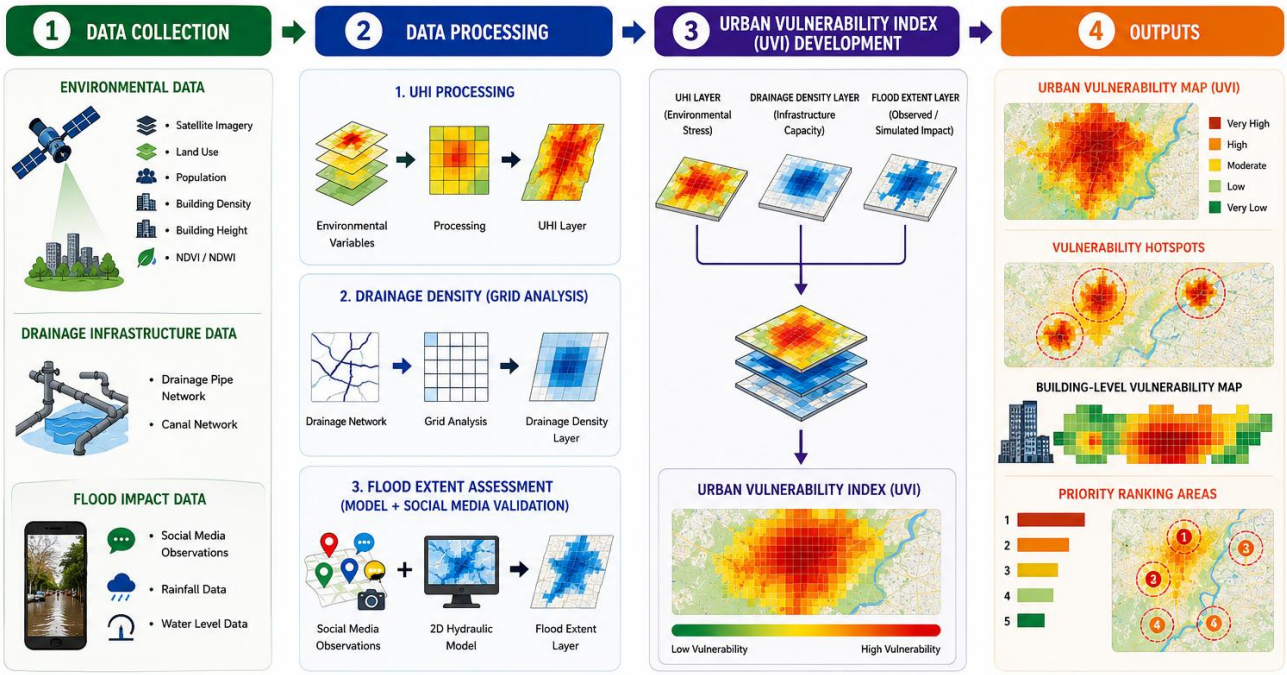

Figure 1. Research framework for urban vulnerability assessment under environmental and flood-related stressors.

2.2. Study Area and Spatial Characteristics

Bangkok, Thailand, is located in an Aw, Tropical Savanna climate under the Koppen classification system with an average annual rainfall of around 1700 mm and average annual temperature of 28.9 °C. Localized flooding within the metropolitan area of Bangkok is common, e.g., [60,61]. City population stood at 5.42 million in 2025 (although the

metropolitan region population is approximately 17.4 million), and with 5300 people/km², it has a population density similar to Los Angeles [62].

Our specific study area covers the Ratchadaphisek–Phahonyothin–Kasetsart Intersection flood management area, designated as one of the enclosed flood management areas under the Bangkok Metropolitan Administration (Figure 2). The area extends across Chatuchak, Bang Sue, Din Daeng, and Huai Khwang districts and covers approximately 36.760 km² [63]. The area is characterized by dense urban development, extensive impervious surfaces [64,65], and an interconnected drainage system consisting of subsurface drainage pipes and open urban waterways/canals [63]. These conditions influence runoff generation, drainage performance, and flood response, making the area suitable for assessing urban vulnerability through the integration of environmental stress, drainage density, and flood-related information. The area was selected because it is a designated BMA flood management area with recurrent flooding at well-known locations (Table 1), a documented network of drainage pipes and canals, and water level monitoring stations that allowed the hydraulic model to be calibrated and validated [63].

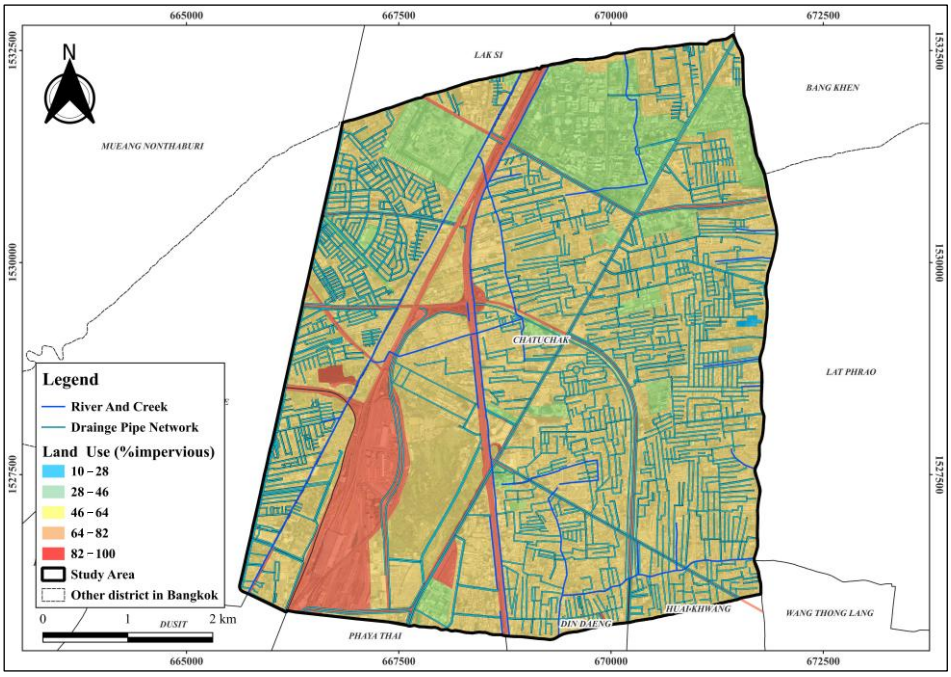

Figure 2. Spatial characteristics of the study area showing land imperviousness and drainage network within the flood management area.

Table 1. Social media-derived flood observations.

Location	Facebook Posts	X (Twitter) Posts	News Reports	Total Observations
Songkhro Municipality–New Prachanivet Market	3	1	1	5
Vibhavadi Road	2	2	1	5
Ratchayothin Intersection	4	2	1	7
Ratchadaphisek Road (Ratchada Area)	5	3	2	10
Lat Phrao Intersection	4	2	1	7
Kamphaeng Phet 2 Road	2	1	1	4
Kamphaeng Phet 1 & 4 Roads	3	2	1	6
Lat Phrao Road	3	2	1	6

2.3. Data Collection

2.3.1. UHI-Related Environmental Stress

Urban Heat Island (UHI) information was developed to represent environmental stress conditions associated with urban surface characteristics. To characterize spatial variations in UHI-related environmental stress, multiple environmental and urban indicators were integrated, including satellite-derived Land Surface Temperature (LST), land use, population distribution, building density, building height, Normalized Difference Vegetation Index (NDVI), and Normalized Difference Water Index (NDWI) [66–69].

In this study, UHI-related environmental stress was represented using a composite indicator integrating thermal, environmental, and urban development variables. Rather than directly quantifying atmospheric or surface UHI intensity from temperature observations alone, the resulting index was designed to characterize UHI-related environmental stress associated with urbanization, vegetation conditions, and built-environment characteristics across the study area. To avoid confusion with the conventional definition of the urban heat island (the temperature difference between an urban area and its rural surroundings), the term "UHI" in this paper refers exclusively to this composite UHI-related environmental stress index and not to atmospheric or surface UHI intensity. Because only one of its seven components (LST) is a direct thermal measurement, the index should be interpreted primarily as an indicator of urbanization-related surface and built-environment stress that includes a thermal component, rather than as a measure of the thermal environment itself. For clarity, this composite is hereafter referred to as the UHI-related environmental stress index (abbreviated as the UHI index in equations and tables), and it is not described as UHI intensity.

LST was derived from Landsat 8 TIRS Band 10 using the Landsat Collection 2 Level-2 surface temperature product (ST_B10) in the Google Earth Engine. Cloud and cloud-shadow pixels were masked using the QA_PIXEL band, the scaled values were converted to degrees Celsius, and all valid scenes acquired between 2020 and 2025 were averaged to produce a five-year mean LST map. Band 10 has a native resolution of 100 m and is distributed resampled to 30 m. NDVI and NDWI were derived from Sentinel-2 MSI surface reflectance imagery (10 m) as five-year (2020–2025) mean composites, with NDVI = (B8 − B4)/(B8 + B4) and NDWI = (B3 − B8)/(B3 + B8). Sentinel-2 was not used for LST because it has no thermal infrared band. Land use data (2022) were obtained from the BMA Department of City Planning and Urban Development, and population data (2022) from the Department of Provincial Administration. The data sources, dates and native resolutions of all inputs are listed in Table A1 (Appendix A), while urban and demographic datasets were obtained from government sources [10,11]. Because the collected datasets were available at different spatial resolutions and certain variables could only be reliably processed at a maximum spatial unit of 100 × 100 m, all datasets were standardized into a common grid framework with a spatial resolution of 100 × 100 m prior to analysis [70,71]. This harmonization process was conducted to ensure spatial consistency, reduce scale-related bias, and enable direct comparison and integration among variables in the subsequent UHI assessment [72].

Each variable was converted to the 100 × 100 m grid as follows. Continuous raster variables (LST, NDVI and NDWI) were aggregated by taking the mean of the pixels within each grid cell. Population density was assigned to grid cells by areal weighting of the administrative-unit population in proportion to residential building area. Building density was calculated as the total building footprint area within each cell divided by the cell area, and building height as the footprint-area-weighted mean height of the buildings in the cell. Land use, a categorical variable, was converted to a numerical land use intensity score by assigning ordinal scores from 1 (water and green space) to 5 (high-density

commercial) and computing the area-weighted mean score within each cell. Drainage density and flood depth were gridded as described in Sections 2.3.2 and 2.3.3.

To ensure comparability among variables with different units and value ranges, all input factors were standardized using Z-score normalization [73]:

$$z_i = \frac{X_i - \bar{X}}{S.D.} \quad (1)$$

where

z_i = standardized value of variable i,

X_i = original value,

$S.D.$ = standard deviation.

The standardized variables were subsequently integrated to generate a composite UHI-related environmental stress index [74]:

$$UHI - related\ environmental\ stress\ index = \sum_{i=1}^{n} w_i\, z_i \quad (2)$$

or expressed as

$$UHI = (w_1 z_{LST}) + (w_2 z_{LU}) + (w_3 z_{POP}) + (w_4 z_{BD}) + (w_5 z_{BH}) + (w_6 z_{NDVI}) + (w_7 z_{NDWI}) \quad (3)$$

where

w_i = weighting coefficient assigned to each variable,

$\sum w_i$ = 1, and

z_i = standardized value of each input factor.

Variables positively associated with urban heat conditions, including LST, land use intensity (LU), population density (POP), building density (BD), and building height (BH), contributed positively to the UHI-related Environmental Stress Index. In this study, population density was incorporated as an indicator of urban development intensity and human concentration rather than as a socioeconomic vulnerability variable. Conversely, NDVI and NDWI were considered mitigating indicators because vegetation cover and surface water generally contribute to reducing urban heat accumulation and therefore contributed inversely to the index [10,75,76]. Due to the absence of established evidence supporting differential importance among the selected indicators, equal weighting was adopted, assigning identical weights to all variables [77]. Pairwise Pearson correlation coefficients among the seven indicators, calculated across all 100 × 100 m grid cells, are given in Table A2 (Appendix A). All correlations had the expected signs. The strongest correlations were between building density and NDVI (r = −0.78), land use intensity and building density (r = 0.76), and land use intensity and NDVI (r = −0.72); no pair exceeded $|r| = 0.8$, a threshold often used to flag redundant indicators. These indicators nevertheless share common urbanization drivers, which can lead to double counting in composite indices [77], so that, under equal weighting, built-up intensity and vegetation loss carry more combined influence in the index than the nominal weights suggest. All seven indicators were therefore retained and this shared influence is taken into account when interpreting the UHI index.

The classification scheme was used to facilitate the interpretation of spatial variations in UHI-related environmental stress across the study area. The resulting classes represent relative differences in environmental stress conditions and provide a basis for subsequent spatial comparison and integration within the Urban Vulnerability Index (UVI).

The resulting UHI dataset was classified into relative stress classes (shown in Figure 3) and used as the environmental stress layer for subsequent integration with drainage density and flood-related information in the Urban Vulnerability Index (UVI) assessment.

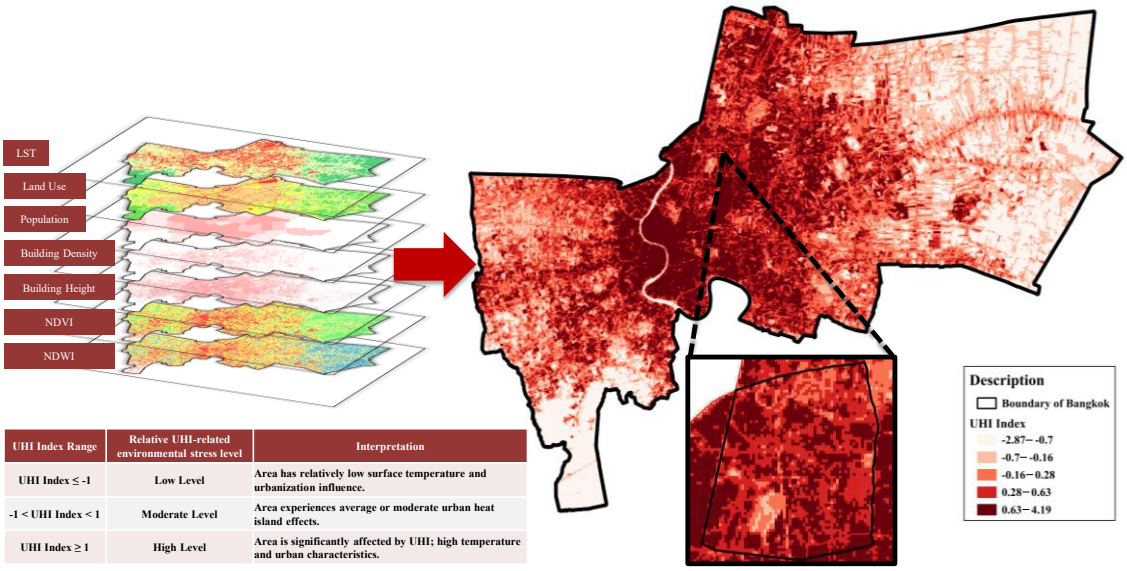

UHI Index Range	Relative UHI-related environmental stress level	Interpretation
UHI Index ≤ -1	Low Level	Area has relatively low surface temperature and urbanization influence.
-1 < UHI Index < 1	Moderate Level	Area experiences average or moderate urban heat island effects.
UHI Index ≥ 1	High Level	Area is significantly affected by UHI; high temperature and urban characteristics.

Figure 3. Spatial distribution of the UHI-related environmental stress derived from integrated urban and environmental indicators.

2.3.2. Drainage Infrastructure Data

Data were collected to represent the availability of drainage infrastructure within the study area, with the dataset consisting of drainage pipe networks and urban waterways, including rivers and canals, obtained from governmental spatial databases [63,78]. Drainage density was calculated as the total length of drainage infrastructure within each grid cell divided by the corresponding grid area. The resulting indicator represents the spatial concentration of drainage networks and was used as a proxy for drainage service availability and stormwater conveyance potential. Urban drainage density (and even roadway networks) has been used successfully as a geospatial proxy in other studies when detailed hydraulic data are limited [79–81]. The drainage system within the study area is characterized by a dense network of drainage pipes distributed across highly urbanized zones, particularly along major transportation corridors and developed areas (Figure 2). To calculate drainage density, the drainage lines were intersected with the 100 × 100 m grid, and the lengths of all line segments falling within each cell were summed and divided by the cell area. Pipes and open canals were treated equivalently, i.e., their lengths were summed without weighting. Because open canals generally convey much larger flows than individual pipes, this equal treatment is a simplification, and drainage density is therefore interpreted only as a proxy for drainage infrastructure availability, not as a measure of hydraulic capacity.

To support spatial analysis, drainage network data were processed within the same 100 × 100 m grid framework used in the UHI-related environmental stress analysis [82,83]. Drainage density was subsequently calculated to represent the spatial concentration of drainage infrastructure within each grid cell. Areas with lower drainage density were interpreted as having relatively less drainage infrastructure and potentially higher sensitivity to flood accumulation during extreme rainfall events [23,84]. It should be noted that drainage density is a geometric proxy for the availability of drainage infrastructure rather than a measure of its hydraulic capacity. It does not account for pipe diameter, invert elevation, slope, sedimentation, blockage or pumping station capacity, all of which affect actual conveyance performance. Some of these hydraulic characteristics are represented in the PCSWMM model used to derive the flood depth layer, but they are not represented in the drainage density layer itself. Where such data are available, operational indicators

such as pipe diameter classes, maintenance and desilting records, and pumping capacity from the BMA Drainage and Sewerage Department could be used to refine this component in future applications.

The resulting drainage density layer in Figure 4 was integrated with UHI-related environmental stress and social media-derived flood observations in the subsequent Urban Vulnerability Index (UVI) assessment.

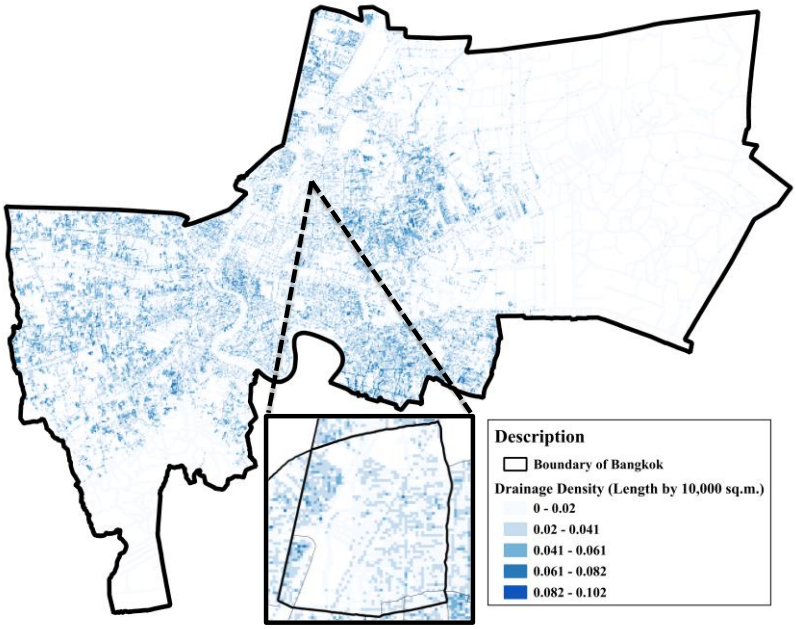

Figure 4. Spatial distribution of drainage density used as a proxy for drainage infrastructure availability within the study area.

2.3.3. Flood-Related Information

Flood-related information was collected from social media platforms to identify locations where flooding was experienced and reported by urban communities during rainfall events. Flood-related information was obtained from publicly available posts, photographs, and location-based reports containing evidence of inundation, traffic disruption, and flood-related impacts within the study area.

The collected records were filtered and validated to remove duplicated, irrelevant, and uncertain observations. Posts containing sufficient spatial information were georeferenced and converted into flood observation points. As summarized in Table 1, a total of 50 flood-related observations were identified from eight frequently reported locations, including Ratchadaphisek Road (Ratchada Area), Ratchayothin Intersection, Lat Phrao Intersection, Kamphaeng Phet 1 and 4 Roads, and Vibhavadi Road. These locations represent areas where flooding was repeatedly documented by local communities during rainfall events.

The identified flood observation points were subsequently used as independent spatial evidence for evaluating flood simulation results generated with a two-dimensional (2D) PCSWMM model (Computational Hydraulics International, Guelph, Ontario, Canada). The hydraulic model was calibrated using the rainfall event of 10 January 2025 (maximum rainfall of 120 mm) and validated using the rainfall event of 9 May 2025 (maximum rainfall of 90 mm) based on observed water level data collected from three monitoring stations within the study area (WL.LPV.01, WL.LPV.04, and WL.BTS.03). Model performance was evaluated using the coefficient of determination (R^2), root mean square error (RMSE), and Nash–Sutcliffe efficiency (NSE), which indicated satisfactory agreement

between observed and simulated water levels. The values of these statistics at each monitoring station are shown in Figure 5 for model calibration and Figure 6 for model validation. Simulated flood extents from selected rainfall events were then compared with social media-derived flood observations. Locations exhibiting consistent agreement between reported flood impacts and simulated inundation areas were used to verify the spatial reliability of the hydraulic model.

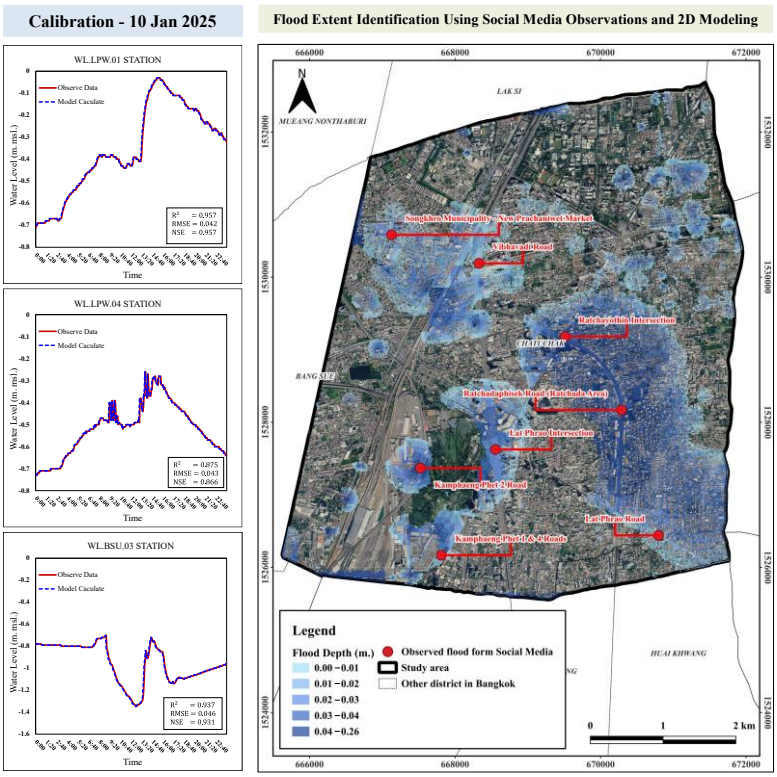

Figure 5. Calibration of the PCSWMM 2D model using observed water level data (**left**) and identification of flood extent through the integration of social media flood observations and hydraulic modeling results (**right**).

As shown in Figures 5 and 6, the majority of social media-derived flood observations were located within areas simulated as inundated by the 2D model, indicating good spatial correspondence between reported flood impacts and model outputs. Based on this agreement, representative flood scenarios were selected and used to generate flood extent and flood depth layers for subsequent vulnerability assessment.

The comparison with social media observations should be regarded as a qualitative spatial plausibility check rather than a formal spatial validation. The 50 observations were concentrated at eight locations, mainly along major roads, and they record only where flooding was reported; they provide no information on locations where flooding did not occur. Contingency-based metrics such as the hit rate combined with false alarm ratio, the critical success index or the F1 score require both flooded and non-flooded reference observations and therefore could not be meaningfully calculated with this dataset [36]. The quantitative performance of the hydraulic model is instead based on the comparison of observed and simulated water levels at three monitoring stations (Figures 5 and 6). Accordingly, the social media comparison supports the plausibility of the simulated flood locations but does not establish the accuracy of the simulated flood extent across the full 36.76 km² study area.

To ensure consistency with other datasets used in the Urban Vulnerability Index (UVI) assessment, the simulated flood depth layer was converted into a 100 × 100 m spatial

grid corresponding to the UHI-related environmental stress and drainage density analyses [82,85–87]. The resulting flood information was subsequently integrated with environmental stress and drainage density indicators to support urban vulnerability assessment and spatial prioritization of flood adaptation measures [42,88,89]. The flood component of the UVI is the simulated flood depth for the 10 January 2025 event (maximum rainfall of 120 mm in the study area), which was also used for model calibration, computed on a 25 × 25 m two-dimensional mesh. For each grid cell, the maximum simulated depth (m) within the cell was used, and cells that were not inundated were assigned a depth of zero. The simulated flood extent, i.e., the proportion of each cell that was inundated, was used to identify flooded cells and for comparison with the social media observations, but it did not enter the UVI. Throughout the paper, "flood depth" therefore refers to the UVI component and "flood extent" to the simulated inundated area.

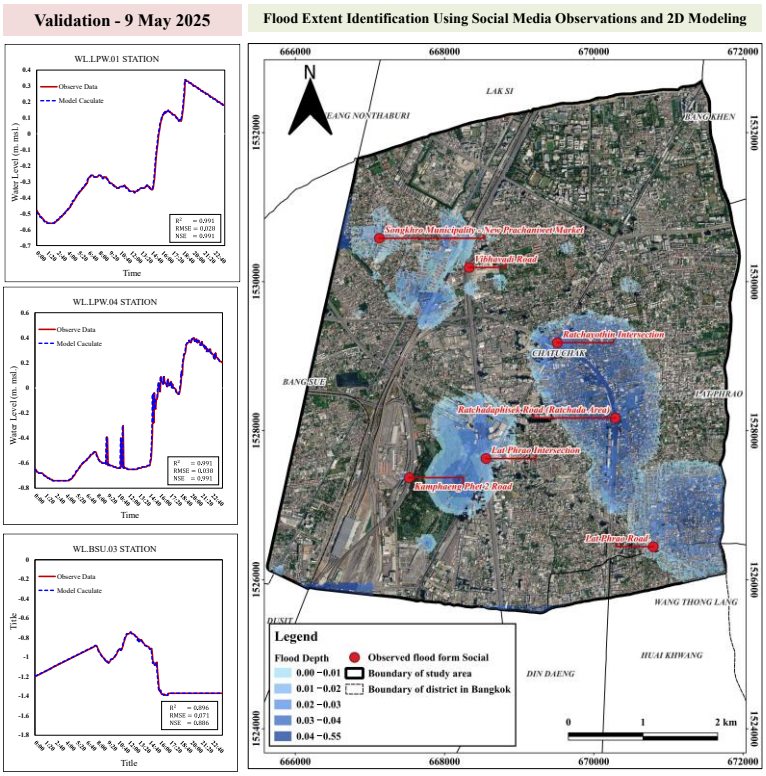

Figure 6. Validation of the PCSWMM 2D model using observed water level data (**left**) and identification of flood extent through the integration of social media flood observations and hydraulic modeling results (**right**).

2.4. Urban Vulnerability Index (UVI)

The Urban Vulnerability Index (UVI) was developed to identify urban areas experiencing the combined influence of environmental stress, drainage limitations, and flood-related information. The index integrates UHI-related environmental stress, drainage density, and flood depth derived from the validated PCSWMM flood simulation to represent different dimensions of urban vulnerability within the study area [90–92].

Prior to integration, all variables were standardized within the same 100 × 100 m spatial grid framework to ensure spatial consistency and comparability among datasets [93,94]. To enable integration among variables with different units and value ranges, all datasets were normalized using Z-score standardization [95–97]. expressed in Equation (1).

The Urban Vulnerability Index was subsequently calculated using weighted overlay analysis [74,98]:

$$UVI = (w_1 z_{UHI}) + (w_2 z_{DD}) + (w_3 z_{Flood}) \quad (4)$$

where

z_{UHI} = standardized UHI-related environmental stress index,

z_{DD} = standardized drainage density,

z_{Flood} = standardized flood depth value, and

w_i = weighting coefficient assigned to each factor.

Equal weighting was applied to all UVI components due to the absence of sufficient evidence supporting differential importance among the selected indicators. This approach reduces subjectivity and ensures that each vulnerability dimension contributes equally to the overall assessment. We acknowledge, however, that equal weighting is itself a value judgement rather than a neutral choice [77]. Data-driven alternatives such as principal component analysis or the entropy weight method derive weights from the statistical variance of the indicators rather than from their importance for vulnerability, whereas expert-based methods such as the Analytic Hierarchy Process and the Delphi method require a structured stakeholder elicitation that was beyond the scope of this study [74,98,99]. Because the UVI has only three components, the contribution of each component to the UVI of any grid cell can be read directly from its standardized score, which keeps the index transparent. The sensitivity of the vulnerability classes and priority rankings to alternative weighting schemes was not evaluated in this study and is acknowledged as a limitation.

Higher UVI values indicate areas characterized by elevated environmental stress, insufficient drainage infrastructure, and higher flood impact conditions, representing zones with greater urban vulnerability [100,101]. The resulting UVI values were classified using the Standard Deviation classification method to represent relative differences in vulnerability conditions across the study area. Five vulnerability classes were subsequently defined, ranging from Very Low to Very High, based on deviations from the mean UVI value. This classification approach facilitates the identification of areas exhibiting relatively higher or lower vulnerability within the study area and supports spatial prioritization for adaptation planning. Because higher drainage density indicates greater availability of drainage infrastructure, the standardized drainage density was reverse-coded, i.e., multiplied by −1 before the equal weights were applied, which is equivalent to a negative coefficient in Equation (4), so that, consistent with Table 2, lower drainage density increases the UVI. NDVI and NDWI were reverse-coded in the same way in Equation (3). The direction of every indicator is listed in Table A1.

Table 2. Relationship between UVI components and vulnerability conditions.

Factor	Z-score Condition	Interpretation	Influence on UVI
UHI-related environmental stress	High (+)	High environmental stress	Increase UVI
UHI-related environmental stress	Low (−)	Low environmental stress	Decrease UVI
Drainage Density	High (+)	High drainage infrastructure availability	Decrease UVI
Drainage Density	Low (−)	Limited drainage infrastructure	Increase UVI
Flood Depth	High (+)	Greater flood depth	Increase UVI
Flood Depth	Low (−)	Shallower flood depth	Decrease UVI

3. Results & Discussion

3.1. Spatial Distribution of the Urban Vulnerability Index (UVI)

The spatial distribution of the Urban Vulnerability Index (UVI) across the study area is presented in Figure 7, while the corresponding area statistics for each vulnerability class are summarized in Table 3. The calculated UVI values ranged from −1.50 to 2.30, indicating substantial spatial variability in urban vulnerability throughout the study area. Because the UVI is a weighted sum of standardized scores, it has no fixed theoretical minimum or maximum. With equal weights of 1/3, the UVI equals the mean of the three standardized components, so a value of 0 corresponds to average conditions in the study area, and all values are interpreted relative to that mean.

Table 3. Area and percentage of Urban Vulnerability Index classes within the study area.

UVI Class	Area (km²)	Percentage (%)
Very Low (≤−0.64)	7.28	19.80
Low (−0.64–(−0.42))	6.74	18.34
Moderate (−0.42–(−0.22))	6.66	18.12
High (−0.22–0.01)	6.18	16.81
Very High (>0.01)	9.90	26.93
Summary	36.76	100.00

The classification results revealed that the Very High vulnerability class occupied the largest proportion of the study area, covering 9.90 km² (26.93%), followed by the Very Low vulnerability class, which accounted for 7.28 km² (19.80%) (Table 3). The Low, Moderate, and High vulnerability classes covered 6.74 km² (18.34%), 6.66 km² (18.12%), and 6.18 km² (16.81%), respectively. Overall, areas classified as Moderate to Very High vulnerability occupied approximately 61.86% of the study area, indicating that a large proportion of the urban landscape is exposed to combined environmental and flood-related pressures.

Spatially, elevated UVI values were distributed throughout much of the study area, with several concentrated clusters observed within the central and eastern portions of the flood management zone (Figure 7). These areas generally corresponded to locations characterized by relatively high UHI-related environmental stress, limited drainage infrastructure, and significant flood impacts derived from the validated flood simulation results. The widespread occurrence of high-vulnerability zones suggests that vulnerability is not confined to isolated flood-prone locations but is influenced by the cumulative effects of environmental stress, drainage conditions, and flood exposure.

In contrast, areas classified as Very Low and Low vulnerability were distributed as fragmented patches across the study area. Several larger low-vulnerability zones were observed in the western-central portion of the study area, where comparatively lower environmental stress and more favorable drainage conditions were present. The discontinuous distribution of these areas indicates that favorable environmental and infrastructure conditions are relatively limited within the highly urbanized landscape. Socioeconomic indicators would help to interpret these patterns, for example by showing whether residents of the remaining low-vulnerability areas also have greater capacity to prepare for and recover from flooding; their inclusion is identified as future work (Section 5).

The spatial patterns observed in Figure 7 highlight the importance of considering multiple dimensions of vulnerability simultaneously. Areas exhibiting elevated environmental stress, constrained drainage conditions, and significant flood impacts consistently produced higher UVI values than surrounding locations. By integrating these factors into a single indicator, the UVI provides a comprehensive representation of urban

vulnerability and facilitates the identification of priority areas for flood adaptation, infrastructure improvement, and urban resilience planning.

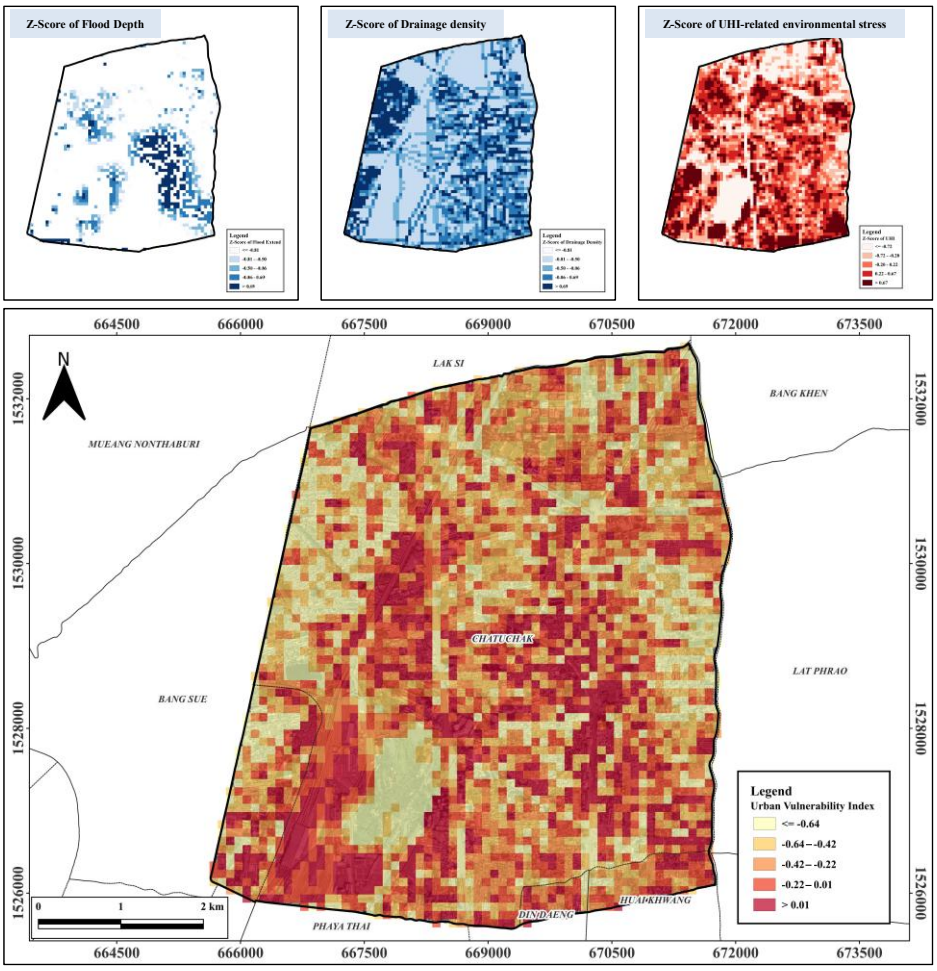

Figure 7. Spatial distribution of the Urban Vulnerability Index (UVI) derived from UHI-related environmental stress, drainage density, and simulated flood depth.

3.2. Spatial Prioritization of Vulnerable Urban Areas

To support practical decision-making and resource allocation, a spatial prioritization analysis was conducted using locations identified within the highest Urban Vulnerability Index (UVI) category. Although all selected locations were classified as very highly vulnerable, differences in UVI values provided additional insight into the relative severity of vulnerability conditions across the study area. A ranking-based approach therefore was applied to distinguish locations requiring more immediate intervention from those with comparatively lower urgency.

The eight locations evaluated in Table 4 correspond to the frequently reported flood locations identified from social media (Table 1). They were used as named reference sites because they are recognized flood problem areas that are meaningful to local decision-makers. We note that the social media observations did not enter into the UVI calculation. The flood depth component was generated by the PCSWMM model, driven by rainfall input and calibrated against water level records from three monitoring stations, and the social media observations were only used afterwards to check the plausibility of the simulated flood locations. This check informed which simulated rainfall scenario was adopted as representative, but it did not modify the simulated flood extent itself. The UHI-related environmental stress and drainage density components are entirely independent of the social media data. The UVI values at these locations therefore result from the model-

derived flood depth together with the environmental stress and drainage components, rather than from the presence of social media reports. Nevertheless, because the evaluated locations were selected on the basis of social media reports, the ranking in Table 4 should be interpreted as a ranking among known problem sites rather than as an exhaustive search for all priority areas. A grid-based hotspot ranking across the entire study area, independent of reported locations, is recommended for future applications.

The prioritization results are summarized in Table 4. Kamphaeng Phet 1 and 4 Roads were identified as the highest-priority locations, exhibiting the highest UVI value of 1.18, followed by Ratchadaphisek Road (Ratchada Area) and Lat Phrao Intersection with UVI values of 1.13 and 0.88, respectively. These locations represent areas where elevated UHI-related environmental stress, drainage limitations, and significant flood impacts spatially converge, resulting in substantially higher vulnerability levels than the surrounding urban environment.

Table 4. Ranking of priority urban locations within the Very High UVI zone.

Priority Rank	Location	UVI
1	Kamphaeng Phet 1 & 4 Roads	1.18
2	Ratchadaphisek Road (Ratchada Area)	1.13
3	Lat Phrao Intersection	0.88
4	Vibhavadi Road	0.62
5	Ratchayothin Intersection	0.48
6	Kamphaeng Phet 2 Road	0.25
7	Songkhro Municipality–New Prachanivet Market	0.24
8	Lat Phrao Road	0.17

Several major transportation corridors were also ranked among the highest-priority locations, including Vibhavadi Road, Ratchayothin Intersection, and Kamphaeng Phet 2 Road. The concentration of highly vulnerable areas along major transportation routes highlights the influence of urban development intensity and infrastructure exposure on vulnerability patterns. Flood-related disruptions in these corridors will not only affect local accessibility but also broader transportation connectivity, economic activities, and emergency response operations during extreme rainfall events.

In addition to transportation corridors, Songkhro Municipality–New Prachanivet Market and Lat Phrao Road, were identified within the priority list. Although these locations exhibited lower UVI values relative to the highest-ranked areas, they remained within the very high vulnerability category. Their inclusion indicates that vulnerability is distributed across different urban functions, including commercial, residential, and transportation-related areas, rather than being concentrated within a single type of urban setting.

The prioritization results further demonstrate that vulnerability conditions vary considerably even within areas classified under the same vulnerability class. For example, UVI values ranged from 0.17 at Lat Phrao Road to 1.18 at Kamphaeng Phet 1 and 4 Roads, indicating substantial differences in the combined effects of environmental stress, drainage infrastructure, and flood impacts. This variation highlights the importance of ranking individual locations rather than relying solely on vulnerability classes when establishing intervention priorities.

The prioritization results are specific to the 100 × 100 m spatial grid adopted in this study, which was selected to ensure consistency among the integrated datasets. Although the proposed framework can be applied at different spatial resolutions, the resulting vulnerability patterns and priority rankings may vary depending on the scale of analysis. Future studies may further investigate the sensitivity of vulnerability assessments to alternative grid sizes and spatial aggregation schemes.

Overall, the proposed prioritization framework extends conventional vulnerability mapping by identifying specific locations where multiple stressors converge and where adaptation measures may generate the greatest benefits. The resulting priority zones provide a practical basis for targeted drainage improvement, flood mitigation measures, green infrastructure implementation, and broader urban resilience planning. By integrating environmental stress indicators, drainage characteristics, and simulated flood depth, the framework supports more effective allocation of resources toward areas facing the greatest combined vulnerability.

3.3. Building-Level Vulnerability Assessment

To further support local-scale planning and risk reduction strategies, the Urban Vulnerability Index (UVI) was integrated with building footprint data [102] to evaluate vulnerability conditions at the individual building level [103]. Building vulnerability classes were assigned through spatial overlay analysis between building footprints and the 100 × 100 m UVI grid framework. Each building was assigned to the vulnerability value of the grid cell in which it was located. Buildings that overlayed in more than one grid cell were assigned the UVI value of the cell containing the largest share of the building footprint area. The assessment was based on the horizontal spatial relationship between building footprints and UVI grid cells, whereas first-floor elevation and building-specific structural characteristics were not incorporated due to data limitations. Consequently, all buildings within the same grid cell receive the same vulnerability class, even though ground floor elevation, micro-topography and building use can vary within a 100 × 100 m cell. A building with an elevated ground floor may be less vulnerable than its grid class suggests, whereas a building with a basement or a ground floor below road level may be more vulnerable. The building-level results should therefore be interpreted as the exposure of each building to grid-level vulnerability conditions rather than as an assessment of the vulnerability of individual structures and they are best used as a screening tool to identify where more detailed building surveys are needed. The resulting assessment classified a total of 77,102 buildings into five vulnerability categories (Table 5 and Figure 8). Moderate vulnerability accounted for the largest proportion, comprising 16,381 buildings (21.25%), followed by Very High vulnerability with 15,387 buildings (19.96%). Buildings classified as High and Very High vulnerability collectively accounted for 30,394 buildings, representing approximately 39.42% of the total building stock within the study area.

The spatial distribution of building vulnerability revealed considerable heterogeneity across the urban landscape. Buildings classified as High and Very High vulnerability were predominantly concentrated within densely developed urban zones, particularly along major transportation corridors and commercial areas. These locations generally corresponded to areas characterized by elevated UHI-related environmental stress, extensive impervious surface coverage, limited drainage infrastructure, and significant flood impacts identified from the simulated flood depth. The concentration of highly vulnerable buildings within these environments suggests that multiple vulnerability factors operate simultaneously and amplify potential flood-related consequences. In future work, the PCSWMM 2D results could be projected onto street-level imagery, for example in Google Earth, to illustrate expected flood conditions at individual buildings and to support a preliminary visual interpretation of the results with local stakeholders.

In contrast, buildings classified as Very Low and Low vulnerability were more frequently observed in areas exhibiting relatively lower environmental stress and more favorable drainage conditions. Although these classes collectively represented approximately 39.33% of all buildings, their spatial distribution remained fragmented and scattered throughout the study area. This pattern indicates that favorable environmental and

infrastructure conditions are limited within the highly urbanized setting and often are surrounded by areas exhibiting higher vulnerability levels.

The enlarged views presented in Figure 8 further demonstrate the heterogeneous nature of vulnerability at the neighborhood scale. Buildings located in close proximity frequently exhibited different vulnerability levels, reflecting localized variations in environmental stress, drainage characteristics, and flood exposure. These findings highlight the importance of high-resolution spatial assessment, as vulnerability conditions may vary substantially even within the same neighborhood.

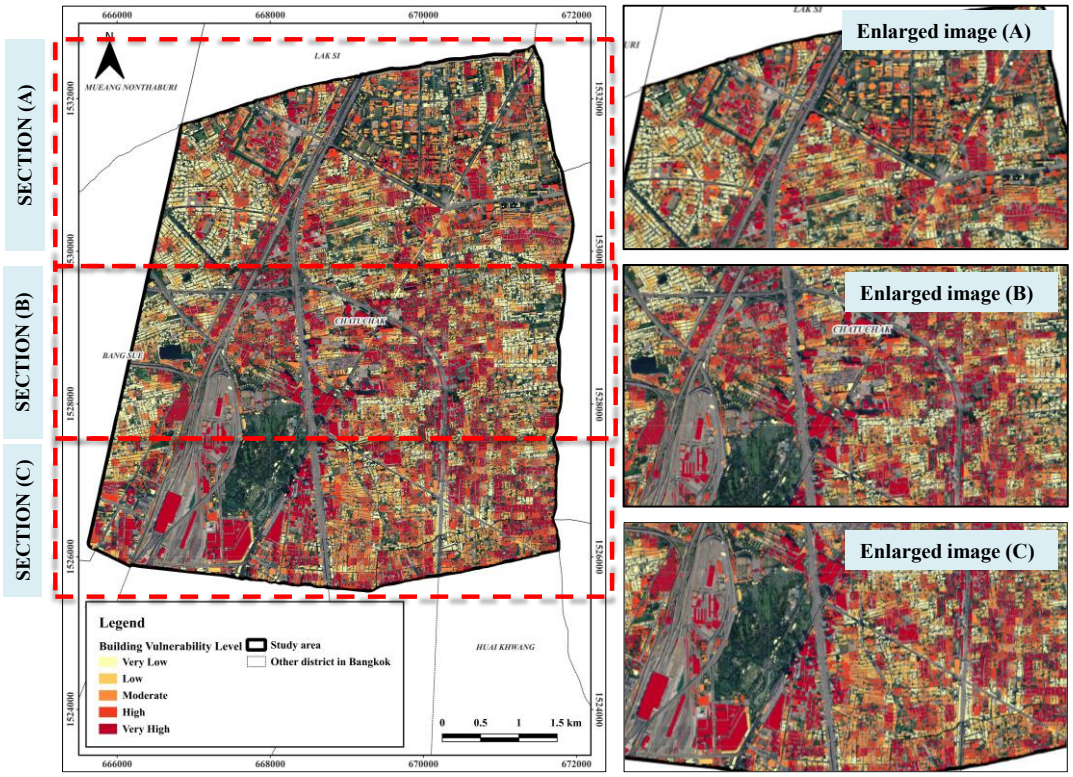

Figure 8. Building-level vulnerability assessment derived from the Urban Vulnerability Index (UVI), showing the spatial distribution of vulnerability classes and enlarged views of selected urban areas, which is divided into three sections. Enlarged views of each section are shown on the right: (A) Section A, the northern part of the study area, bordering Lak Si; (B) Section B, the central part, covering the Chatuchak area; (C) Section C, the southern part, including the railway yard and adjacent green space.

From a practical perspective, the building-level vulnerability map provides information directly applicable to urban planning and adaptation strategies. Buildings classified as High and Very High vulnerability may be prioritized for flood preparedness planning, drainage improvement programs, resilience enhancement measures, and emergency response management. By linking environmental stress, drainage infrastructure, and flood impacts to individual buildings the proposed framework extends conventional area-based assessments and provides a more detailed representation of vulnerability at the scale where flood impacts are ultimately experienced. Buildings in the High and Very High classes are also likely to face combined exposure to heat stress and to floodwater, which in dense urban areas may carry pollutants from roads, drains, and canals. Although health and water quality risks were not assessed in this study, the building-level map could be overlaid with water quality and public health data in future work to identify buildings, particularly residential and commercial buildings in districts such as Chatuchak and Din Daeng, where these exposures coincide.

Table 5. Number of Buildings by Urban Vulnerability Class.

Vulnerability Class	Number of Buildings	Percentage (%)
Very Low	15,145	19.64
Low	15,182	19.69
Moderate	16,381	21.25
High	15,007	19.46
Very High	15,387	19.96
Total	77,102	100.00

4. Discussion

4.1. Environmental Stress as a Component of Urban Vulnerability

The results demonstrate that urban vulnerability is influenced not only by flood occurrence but also by broader environmental conditions. Areas exhibiting elevated UHI-related environmental stress generally corresponded to highly urbanized environments characterized by extensive impervious surfaces, dense built-up development, and limited green spaces. These conditions have been widely recognized as indicators of accumulated environmental stress and reduced urban resilience [14,104]. In this study, UHI was used as a proxy indicator of environmental stress rather than a direct measure of atmospheric heat island intensity. The integrated UHI index was designed to capture the combined influence of thermal conditions, urban development characteristics, vegetation conditions, and surface properties that collectively reflect environmental pressure within the urban landscape. Because six of the seven input variables describe urban form, land cover, and population rather than temperature, the index reflects urbanization intensity at least as much as the thermal environment. Its contribution to the UVI should therefore be interpreted as the effect of intensive urban development, including impervious surfaces, limited vegetation, and dense buildings, which affects both heat accumulation and runoff generation, rather than as the effect of heat alone.

The integration of UHI into the Urban Vulnerability Index (UVI) provided additional information beyond conventional flood hazard assessments. While flood extent identifies where inundation occurs, UHI reflects underlying urban conditions that may exacerbate environmental pressures and reduce adaptive capacity [105]. Consequently, areas experiencing both elevated UHI-related environmental stress and flood impacts tended to exhibit higher vulnerability levels than areas affected by flooding alone. This finding supports the growing recognition that urban vulnerability emerges through the interaction of multiple environmental stressors rather than a single hazard event [106,107].

4.2. Integrating Social Media Observations and Hydraulic Modeling

This study highlights the potential of combining citizen-generated observations with hydraulic modeling for urban flood assessment. Social media provided valuable information on locations where flooding was directly experienced and reported by local communities, enabling the identification of flood-prone locations that may not be fully represented by conventional monitoring systems [28,95].

Rather than using social media observations as a standalone flood mapping dataset, the observations were employed as independent spatial evidence to evaluate simulated flood extents generated by the PCSWMM 2D model. This integration improved confidence in the selected flood scenarios and facilitated the identification of representative flood extent conditions within the study area. The results demonstrate that social media can serve as a practical complementary data source for flood model evaluation, particularly in urban environments where monitoring data are limited [36,108].

However, the social media dataset used in this study also has important limitations. First, the sample was small, with 50 observations from eight locations. Second, the observations were spatially biased: reports were concentrated along major roads, intersections, and commercial areas, where traffic disruption is visible to many people, whereas flooding in residential side streets (sois), lower-income communities and less-frequented areas is likely to be under-reported because of differences in smartphone use, social media activity, and the newsworthiness of local flooding. Third, the absence of reports does not indicate the absence of flooding. As a result, the social media comparison supports the plausibility of the simulated flood extent at frequently reported locations but provides little information on model performance elsewhere in the study area, and it may have contributed to the concentration of evaluated priority sites along major corridors (Section 3.2). Future applications should triangulate crowd-sourced observations with official BMA flood complaint records (for example, reports submitted through the Traffy Fondue citizen reporting platform), water level sensors, and CCTV observations, which would reduce reporting bias and provide both flooded and non-flooded observations for quantitative evaluation.

The approach also illustrates how citizen-generated information can contribute to more dynamic and spatially explicit flood assessments. As social media usage continues to increase, these data sources may become increasingly valuable for supporting urban flood monitoring, model validation, and disaster management applications [109,110] . Future developments may further enhance these capabilities through integration with emerging urban sensing technologies, including Internet of Things (IoT) sensors, CCTV camera networks, and web-based monitoring platforms. Combining citizen-generated observations with automated sensing systems may improve the timeliness, spatial coverage, and reliability of flood information, thereby supporting more effective real-time flood monitoring, early warning, and urban disaster management [111,112].

4.3. Implications for Urban Flood Adaptation and Spatial Prioritization

One of the main contributions of this study is the integration of environmental stress, drainage infrastructure, and flood-related information within a unified geospatial framework for urban vulnerability assessment and adaptation prioritization, moving beyond traditional flood hazard mapping. While conventional flood assessments typically identify areas exposed to inundation, the proposed framework identifies locations where environmental stress, drainage limitations, and flood-related pressures converge simultaneously.

The prioritization results revealed that several major transportation corridors and commercial areas, including Kamphaeng Phet 1 & 4 Roads, Ratchadaphisek Road, and Lat Phrao Intersection, exhibited substantially higher UVI values than surrounding areas. These locations represent critical urban zones where disruptions may affect transportation accessibility, economic activities, and emergency response operations during flood events. Consequently, these areas may warrant greater attention in future adaptation planning.

From a practical perspective, the identified priority zones provide a basis for targeted interventions, including drainage system enhancement, green infrastructure implementation, urban heat mitigation measures, and flood preparedness programs. In areas characterized by limited drainage density, adaptation strategies may extend beyond conventional drainage expansion and incorporate nature-based solutions (NbS), such as urban green spaces, bioswales, permeable surfaces, and stormwater retention systems, to improve runoff management and enhance urban resilience. The proposed framework therefore provides a decision-support tool that can assist urban planners and local authorities in allocating limited resources more effectively and strengthening urban resilience under increasing climate and urbanization pressures [113].

Because the UVI is the sum of three standardized components, the dominant driver at each priority location can be identified from its component scores, and adaptation

measures can be matched to that driver rather than applied as a generic checklist. Where a high UVI is driven mainly by low drainage density, priority should be given to extending the drainage network, increasing pipe capacity, and improving connections to canals and pumping stations. Where it is driven mainly by flood depth despite adequate drainage density, the constraint is more likely to lie in downstream conveyance, outfall water levels, or pumping capacity, so hydraulic bottleneck analysis and pump operation should be addressed first. Where it is driven mainly by UHI-related environmental stress, measures that reduce imperviousness and increase vegetation, such as permeable pavements [78], bioswales, green roofs and pocket parks, can reduce both runoff and surface heat. For major transport corridors such as Kamphaeng Phet 1 & 4 Roads and Ratchadaphisek Road, where flooding disrupts traffic and emergency access, these measures should be combined with real-time flood warning and traffic management.

5. Conclusions

This study developed an integrated geospatial framework for assessing urban vulnerability and adaptation priorities by combining environmental stress, drainage density, and flood depth information within a GIS environment. The proposed Urban Vulnerability Index (UVI) enabled the spatial integration of environmental, infrastructure, and flood-related factors to identify vulnerable areas within the Ratchadaphisek–Phahonyothin–Kasetsart Intersection flood management zone.

The results showed marked spatial variability in vulnerability conditions across the study area. Approximately 61.86% of the area was classified within the Moderate to Very High vulnerability classes, indicating that vulnerability-related pressures are widely distributed throughout the urban landscape. Areas with high UVI values were generally associated with elevated environmental stress, limited drainage infrastructure, and greater flood depth, suggesting that these factors collectively contribute to increasing vulnerability.

Priority ranking analysis identified Kamphaeng Phet 1 and 4 Roads, Ratchadaphisek Road (Ratchada Area), and Lat Phrao Intersection as the locations exhibiting the highest vulnerability levels. In addition, the building-level assessment revealed substantial variation in vulnerability among individual buildings, even within the same neighborhood, highlighting the importance of high-resolution spatial analysis for local-scale planning.

The integration of earth observation data, drainage infrastructure information, hydraulic modeling outputs, and social media observations provided a broader perspective on urban vulnerability than flood hazard assessment alone. Rather than focusing solely on flood occurrence, the proposed framework identified locations where environmental stress, drainage constraints, and flood-related pressures occur simultaneously.

Several limitations should be acknowledged. Flood observations derived from social media provide valuable spatial information on reported flood conditions; however, they may not capture all flood events and remain influenced by user reporting behavior, data availability, and the spatial distribution of active users. Consequently, reported flood locations may not fully represent the complete extent of flooding across the study area. Future studies may benefit from integrating additional data sources, such as official reporting platforms, IoT-based monitoring systems, CCTV networks, and other real-time sensing technologies to improve the coverage and reliability of flood-related information. In addition, the social media dataset was small (50 observations from eight locations) and concentrated along major roads, and the hydraulic model was calibrated and validated using only one rainfall event each (10 January 2025 and 9 May 2025) at three water level stations. These are the main methodological constraints on the robustness of the flood depth component, and the results should be interpreted with them in mind.

In addition, equal weighting was applied during the development of the Urban Vulnerability Index (UVI), assuming identical contributions from all indicators. Although this

approach provides methodological transparency and simplicity, it may not fully reflect the relative importance of individual factors under different urban conditions. Future research may incorporate alternative weighting approaches and additional socioeconomic and demographic indicators, including population characteristics, socioeconomic conditions, and community sensitivity factors, to provide a more comprehensive representation of urban vulnerability. The sensitivity of the results to the weighting scheme, for example, using entropy-, PCA- or AHP-derived weights, was not tested and should be evaluated in future studies. Furthermore, drainage density represents the availability of the drainage network rather than its hydraulic capacity, and the building-level assessment does not account for ground floor elevation or structural characteristics. Because socioeconomic sensitivity and community adaptive capacity were not included, the UVI represents physical flood vulnerability and should not be interpreted as a measure of social or community vulnerability. Moving forward, we can consider inclusion of other geospatially explicit indicators, including air quality, noise, greenspace quality and extent, transportation patterns, and demographics such as income status within the framework demonstrated herein.

Overall, the proposed framework provides a practical basis for identifying vulnerable urban areas and supporting adaptation planning in highly urbanized environments. The approach also may be applied in other cities where environmental stress and flood-related pressures interact to influence urban vulnerability.

Author Contributions: Conceptualization, D.C. and R.C.; project administration, D.C.; writing—original draft preparation, D.C. and R.C.; writing—review and editing, D.C., R.C., A.P. and K.N.I.; investigation, R.C., A.P. and K.N.I.; formal analysis, R.C.; data curation, R.C.; visualization, R.C. All authors have read and agreed to the published version of the manuscript.

Funding: This research was supported by Kasetsart University Research and Development Institute, KURDI, for the Development of Early-Career Researchers, Fiscal Year 2025, Grant No. YF(KU)12.68.

Data Availability Statement:. The data presented in this study are available on request from the corresponding author due to (specify the reason for the restriction, for example: due to privacy).

Acknowledgments: The authors gratefully acknowledge financial support from Kasetsart University Research and Development Institute, KURDI, through the Kasetsart University Research Project for the Development of Early-Career Researchers (Grant No. YF(KU)12.68). Appreciation is extended to the Bangkok Metropolitan Administration (BMA) and relevant agencies for providing spatial, drainage infrastructure, and environmental datasets that supported this research.

Conflicts of Interest: The authors declare no conflicts of interest.

Abbreviations

The following abbreviations are used in this manuscript:

UVI	Urban Vulnerability Index
UHI	Urban Heat Island (here, the composite UHI-related environmental stress index)
PCSWMM	Personal Computer Storm Water Management Model
LST	Land Surface Temperature
NDVI	Normalized Difference Vegetation Index
NDWI	Normalized Difference Water Index

Appendix A

Table A1 lists the input datasets, their sources, dates or observation periods, native spatial resolutions, and their direction and weight in the UHI-related environmental stress index (UHI index) and the Urban Vulnerability Index (UVI). Table A2 gives the pairwise correlations among the seven UHI indicators.

Table A1. Data inventory of the input datasets and indicators.

Dataset/Indicator	Source	Date or Observation Period	Native Resolution	Use (Direction; Weight)
Land Surface Temperature (LST)	Landsat 8 TIRS Band 10 (Collection 2 Level-2, Google Earth Engine)	2020–2025 (five-year mean)	100 m (distributed at 30 m)	UHI index (+; 1/7)
NDVI	Sentinel-2 MSI surface reflectance	2020–2025 (five-year mean)	10 m	UHI index (−; 1/7)
NDWI	Sentinel-2 MSI surface reflectance	2020–2025 (five-year mean)	10 m	UHI index (−; 1/7)
Land use intensity	BMA Department of City Planning and Urban Development	2022	Vector polygons	UHI index (+; 1/7)
Population density	Department of Provincial Administration (DOPA)	2022	Administrative units	UHI index (+; 1/7)
Building density	Calculated from building footprints [102]	Accessed 15 May 2025	Vector polygons	UHI index (+; 1/7)
Building height	Bangkok Metropolitan Administration (BMA)	2022	Vector polygons	UHI index (+; 1/7)
UHI-related environmental stress index	Composite of the seven indicators above	—	100 × 100 m grid	UVI (+; 1/3)
Drainage network (pipes and canals)	BMA Drainage and Sewerage Department [63,78]	2022	Vector lines	Drainage density in UVI (−; 1/3)
Rainfall and water level	BMA monitoring stations WL.LPV.01, WL.LPV.04, WL.BTS.03	10 January 2025 (calibration); 9 May 2025 (validation)	5-min records	PCSWMM calibration and validation
Flood depth	PCSWMM 2D simulation	10 January 2025 event (maximum rainfall 120 mm)	25 × 25 m mesh	UVI (+; 1/3)
Social media flood observations	Facebook, X (Twitter), online news	Collected after the 10 January 2025 event	50 points at 8 locations	Plausibility check only (not in UVI)
Building footprints	OpenStreetMap [102]	Accessed 15 May 2025	Vector polygons (77,102)	Building-level assignment

Table A2. Pairwise Pearson correlation coefficients (r) among the seven indicators of the UHI index, calculated across all 100 × 100 m grid cells.

Indicator	LST	Land Use	Population Density	Building Density	Building Height	NDVI	NDWI
LST	1.00						
Land use	0.62	1.00					
Population density	0.48	0.55	1.00				
Building density	0.58	0.76	0.68	1.00			
Building height	0.32	0.44	0.46	0.52	1.00		
NDVI	−0.68	−0.72	−0.58	−0.78	−0.38	1.00	
NDWI	−0.42	−0.48	−0.36	−0.50	−0.25	−0.65	1.00

References

1. Shaw, R.; Luo, Y.; Cheong, T.S. *Climate Change 2022: Impacts, Adaptation and Vulnerability*; Cambridge University Press: Cambridge, UK; New York, NY, USA, 2023.
2. UNDRR. *Global Assessment Report on Disaster Risk Reduction (GAR)*; United Nations Office for Disaster Risk Reduction: Geneva, Switzerland, 2022.
3. Lazzarin, T.; Chen, A.S.; Viero, D.P. Beyond Flood Hazard. Mapping the Loss Probability of Pedestrians to Improve Risk Estimation and Communication. *Sci. Total Environ.* **2024**, *912*, 168718. https://doi.org/10.1016/j.scitotenv.2023.168718.
4. Alsaleh, A.R.S.; Alcibahy, M.; Al Momani, D.E.; Al Hashemi, H.; Al Hammadi, A.A.; AlAwadi, K.; Seneviratne, L.; Al Shehhi, M.R. Satellite-Based Soil Texture Mapping Using GLOBAL–LOCAL Spectral Libraries for Flood Hazard Assessment in Arid Regions. *Remote Sens. Appl. Soc. Environ.* **2026**, *42*, 101997. https://doi.org/10.1016/j.rsase.2026.101997.
5. Pakati, S.S.; Shoko, C.; Dube, T. Integrated Flood Modelling and Risk Assessment in Urban Areas: A Review on Applications, Strengths, Limitations and Future Research Directions. *J. Hydrol. Reg. Stud.* **2025**, *61*, 102583. https://doi.org/10.1016/j.ejrh.2025.102583.
6. Anwana, E.O.; Owojori, O.M. Analysis of Flooding Vulnerability in Informal Settlements Literature: Mapping and Research Agenda. *Soc. Sci.* **2023**, *12*, 40. https://doi.org/10.3390/socsci12010040.
7. De Risi, R.; Jalayer, F.; De Paola, F.; Iervolino, I.; Giugni, M.; Topa, M.E.; Mbuya, E.; Kyessi, A.; Manfredi, G.; Gasparini, P. Flood Risk Assessment for Informal Settlements. *Nat. Hazards* **2013**, *69*, 1003–1032. https://doi.org/10.1007/s11069-013-0749-0.
8. Zhou, D.; Zhao, S.; Liu, S.; Zhang, L.; Zhu, C. Surface Urban Heat Island in China's 32 Major Cities: Spatial Patterns and Drivers. *Remote Sens. Environ.* **2014**, *152*, 51–61. https://doi.org/10.1016/j.rse.2014.05.017.
9. Abed, S.A.; Halder, B.; Yaseen, Z.M. Investigation of the Decadal Unplanned Urban Expansion Influenced Surface Urban Heat Island Study in the Mosul Metropolis. *Urban Clim.* **2024**, *54*, 101845. https://doi.org/10.1016/j.uclim.2024.101845.
10. Voogt, J.A.; Oke, T.R. Thermal Remote Sensing of Urban Climates. *Remote Sens. Environ.* **2003**, *86*, 370–384. https://doi.org/10.1016/S0034-4257(03)00079-8.
11. Weng, Q. Thermal Infrared Remote Sensing for Urban Climate and Environmental Studies: Methods, Applications, and Trends. *ISPRS J. Photogramm. Remote Sens.* **2009**, *64*, 335–344. https://doi.org/10.1016/j.isprsjprs.2009.03.007.
12. Wang, J.; Qingming, Z.; Guo, H.; Jin, Z. Characterizing the Spatial Dynamics of Land Surface Temperature–Impervious Surface Fraction Relationship. *Int. J. Appl. Earth Obs. Geoinf.* **2016**, *45*, 55–65. https://doi.org/10.1016/j.jag.2015.11.006.
13. Qiu, R.; Zhan, Q.; Tu, S.; Li, C. Interannual Variability of Surface Urban Heat Islands across Global Cities: Patterns and Climatic Drivers. *Urban Clim.* **2026**, *65*, 102772. https://doi.org/10.1016/j.uclim.2026.102772.
14. Santamouris, M. Recent Progress on Urban Overheating and Heat Island Research. Integrated Assessment of the Energy, Environmental, Vulnerability and Health Impact. Synergies with the Global Climate Change. *Energy Build.* **2020**, *207*, 109482. https://doi.org/10.1016/j.enbuild.2019.109482.
15. Santamouris, M. Regulating the Damaged Thermostat of the Cities—Status, Impacts and Mitigation Challenges. *Energy Build.* **2015**, *91*, 43–56. https://doi.org/10.1016/j.enbuild.2015.01.027.
16. Hussain, M.F.; Meng, X.; Shah, S.F.; Hu, X. Integrating Urban Growth, Environmental Stress and Public Sentiment through a Multifunctionality-Inspired Spatiotemporal Trade-Off Framework: Evidence from Peshawar, Pakistan. *Sustain. Cities Soc.* **2026**, *144*, 107406. https://doi.org/10.1016/j.scs.2026.107406.
17. Steensen, B.M.; Marelle, L.; Hodnebrog, Ø.; Myhre, G. Future Urban Heat Island Influence on Precipitation. *Clim. Dyn.* **2022**, *58*, 3393–3403. https://doi.org/10.1007/s00382-021-06105-z.
18. Dixon, P.G.; Mote, T.L. Patterns and Causes of Atlanta's Urban Heat Island–Initiated Precipitation. *J. Appl. Meteor. Climatol.* **2003**, *42*, 1273–1284.
19. Ngarambe, J.; Joen, S.J.; Han, C.H.; Yun, G.Y. Exploring the Relationship between Particulate Matter, CO, SO_2, NO_2, O_3 and Urban Heat Island in Seoul, Korea. *J. Hazard. Mater.* **2021**, *403*, 123615.
20. Zheng, Z.; Ren, G.; Wang, H.; Dou, J.; Gao, Z.; Duan, C.; Li, Y.; Ngarukiyimana, J.P.; Zhao, C.; Cao, C.; et al. Relationship between Fine-Particle Pollution and the Urban Heat Island in Beijing, China: Observational Evidence. *Bound.-Layer Meteorol.* **2018**, *169*, 93–113.
21. Piracha, A.; Chaudhary, M.T. Urban Air Pollution, Urban Heat Island and Human Health: A Review of the Literature. *Sustainability* **2022**, *14*, 9234.
22. Fletcher, T.D.; Andrieu, H.; Hamel, P. Understanding, Management and Modelling of Urban Hydrology and Its Consequences for Receiving Waters: A State of the Art. *Adv. Water Resour.* **2013**, *51*, 261–279. https://doi.org/10.1016/j.advwatres.2012.09.001.

23. Butler, D.; Digman, C.; Makropoulos, C.; Davies, J.W. *Urban Drainage*, 4th ed.; CRC Press: Boca Raton, FL, USA, 2018; ISBN 978-1-351-17430-5.
24. Shuster, W.D.; Bonta, J.; Thurston, H.; Warnemuende, E.; Smith, D.R. Impacts of Impervious Surface on Watershed Hydrology: A Review. *Urban Water J.* **2005**, *2*, 263–275. https://doi.org/10.1080/15730620500386529.
25. Radhakrishnan, M.; Pathirana, A.; Ashley, R.M.; Gersonius, B.; Zevenbergen, C. Flexible Adaptation Planning for Water Sensitive Cities. *Cities* **2018**, *78*, 87–95. https://doi.org/10.1016/j.cities.2018.01.022.
26. Songchon, C.; Wright, G.; Beevers, L. The Use of Crowdsourced Social Media Data to Improve Flood Forecasting. *J. Hydrol.* **2023**, *622*, 129703. https://doi.org/10.1016/j.jhydrol.2023.129703.
27. Ahmad, K.; Pogorelov, K.; Riegler, M.; Ostroukhova, O.; Halvorsen, P.; Conci, N.; Dahyot, R. Automatic Detection of Passable Roads after Floods in Remote Sensed and Social Media Data. *Signal Process. Image Commun.* **2019**, *74*, 110–118. https://doi.org/10.1016/j.image.2019.02.002.
28. Khandokar, A.; Mason, J.B.; Singh, R.; Jahangeer, J.; Lee, J.; Andrews, J.; Jahan, R.N.; Noor, M.A.; Joshi, P.; Nam, Y.; et al. Social Media Adoption in Urban and Rural Flood Risk Management: Evidence from Nebraska's 2019 Flood-Affected Regions. *Hum. Settl. Sustain.* **2026**, *2*, 123–133. https://doi.org/10.1016/j.hssust.2026.03.002.
29. Eilander, D.; Trambauer, P.; Wagemaker, J.; van Loenen, A. Harvesting Social Media for Generation of Near Real-Time Flood Maps. *Procedia Eng.* **2016**, *154*, 176–183. https://doi.org/10.1016/j.proeng.2016.07.441.
30. Arthur, R.; Boulton, C.A.; Shotton, H.; Williams, H.T.P. Social Sensing of Floods in the UK. *PLoS ONE* **2018**, *13*, e0189327. https://doi.org/10.1371/journal.pone.0189327.
31. Cravo, M.; Estima, J.; da Silva, A.R.; Matos, J.; Ricardo, A.M.; Ferreira, R.M.L. Citizen Participation in Flood Risk Management: Usability Insights from the RiverCure Portal. *Int. J. Disaster Risk Reduct.* **2026**, *133*, 105961. https://doi.org/10.1016/j.ijdrr.2025.105961.
32. Sy, B.; Frischknecht, C.; Dao, H.; Consuegra, D.; Giuliani, G. Flood Hazard Assessment and the Role of Citizen Science. *J. Flood Risk Manag.* **2018**, *12*, e12519. https://doi.org/10.1111/jfr3.12519.
33. Fan, C.; Esparza, M.; Dargin, J.; Wu, F.; Oztekin, B.; Mostafavi, A. Spatial Biases in Crowdsourced Data: Social Media Content Attention Concentrates on Populous Areas in Disasters. *Comput. Environ. Urban Syst.* **2020**, *83*, 101514.
34. Zheng, L.; Chen, L.; Long, F.; Liu, J.; Li, L. Reducing Social Media Attention Inequality in Disasters: The Role of Official Media During Rainstorm Disasters in China. *Int. J. Disaster Risk Sci.* **2024**, *15*, 388–403.
35. Zhu, Z.; Tian, Z.; Yin, X. Citizen Flood Imagery Enhances Urban Aftermath Monitoring and Exposes Reporting Inequities. *Commun. Earth Environ.* 2026, 7. https://doi.org/10.1038/s43247-026-04049-y.
36. Assumpção, T.H.; Popescu, I.; Jonoski, A.; Solomatine, D.P. Citizen Observations Contributing to Flood Modelling: Opportunities and Challenges. *Hydrol. Earth Syst. Sci.* **2018**, *22*, 1473–1489. https://doi.org/10.5194/hess-22-1473-2018.
37. Pirasteh, S.; Fang, Y.; Mafi-Gholami, D.; Abulibdeh, A.; Nouri-Kamari, A.; Khonsari, N. Enhancing Vulnerability Assessment through Spatially Explicit Modeling of Mountain Social-Ecological Systems Exposed to Multiple Environmental Hazards. *Sci. Total Environ.* **2024**, *930*, 172744. https://doi.org/10.1016/j.scitotenv.2024.172744.
38. Das, S.; Hazra, S.; Haque, A.; Rahman, M.; Nicholls, R.J.; Ghosh, A.; Ghosh, T.; Salehin, M.; Safra de Campos, R. Social Vulnerability to Environmental Hazards in the Ganges-Brahmaputra-Meghna Delta, India and Bangladesh. *Int. J. Disaster Risk Reduct.* **2021**, *53*, 101983. https://doi.org/10.1016/j.ijdrr.2020.101983.
39. Chakraborty, L.; Rus, H.; Henstra, D.; Thistlethwaite, J.; Scott, D. A Place-Based Socioeconomic Status Index: Measuring Social Vulnerability to Flood Hazards in the Context of Environmental Justice. *Int. J. Disaster Risk Reduct.* **2020**, *43*, 101394. https://doi.org/10.1016/j.ijdrr.2019.101394.
40. Cutter, S.L.; Barnes, L.; Berry, M.; Burton, C.; Evans, E.; Tate, E.; Webb, J. A Place-Based Model for Understanding Community Resilience to Natural Disasters. *Glob. Environ. Change* **2008**, *18*, 598–606. https://doi.org/10.1016/j.gloenvcha.2008.07.013.
41. Irvine, K.; Likitswat, F.; Sahavacharin, A.; Suwanarit, A.; Lertwarapornpong, T.; Chitwatkulsiri, D. The Agrihood Design: Valuation of Ecosystem Services for NbS Visions in Peri-Urban Housing Estate Development, Bangkok, Thailand. *J. Archit. Plan. Res. Stud. (JARS)* **2024**, *21*, 115–140.
42. Meerow, S.; Newell, J.P.; Stults, M. Defining Urban Resilience: A Review. *Landsc. Urban Plan.* **2016**, *147*, 38–49. https://doi.org/10.1016/j.landurbplan.2015.11.011.
43. Liang, X.; Liu, D. Wildfire Risk in Alaska: Spatial Association between Social Vulnerability, Wildfire Hazard, and Wildfire Mitigation Programs. *Landsc. Urban Plan.* **2025**, *258*, 105321. https://doi.org/10.1016/j.landurbplan.2025.105321.

44. Contreras, E.; Veigel, N.; Suda, J.; Kreibich, H.; Cominola, A. Mapping Flood Memory: How Risk Perception and Social Vulnerability Drive Flood Insurance Patterns in the U.S. *Int. J. Disaster Risk Reduct.* **2026**, *141*, 106162. https://doi.org/10.1016/j.ijdrr.2026.106162.
45. Fuchs, S.; Birkmann, J.; Glade, T. Vulnerability Assessment in Natural Hazard and Risk Analysis: Current Approaches and Future Challenges. *Nat. Hazards* **2012**, *64*, 1969–1975. https://doi.org/10.1007/s11069-012-0352-9.
46. Babel, M.S.; Gupta, A.D.; Rivas, A.A.; Evers, M.; Kazama, F.; Nakamura, T.; Stoecker, F. Hydrogeochemical and Isotopic Characterization of Groundwater Salinization in the Bangkok Aquifer System, Thailand. *Environ. Earth Sci.* **2013**, *68*, 749–763. https://doi.org/10.1007/s12665-012-1776-y.
47. Bremard, T. Monitoring Land Subsidence: The Challenges of Producing Knowledge and Groundwater Management Indicators in the Bangkok Metropolitan Region, Thailand. *Sustainability* **2022**, *14*, 10593. https://doi.org/10.3390/su141710593.
48. Chaturongkasumrit, Y.; Techaruvichit, P.; Takahashi, H.; Kimura, B.; Keeratipibul, S. Microbiological Evaluation of Water during the 2011 Flood Crisis in Thailand. *Sci. Total Environ.* **2013**, *463*, 959–967.
49. Chomsri, J.; Sherer, P. Social Vulnerability and Suffering of Flood-Affected People: Case Study of 2011 Mega Flood in Thailand. *Kasetsart J. Soc. Sci.* **2013**, *34*, 491–499.
50. Sanguanklin, N.; McFarlin, B.L.; Park, C.G.; Giurgescu, C.; Finnegan, L.; White-Traut, R.; Engstrom, J.L. Effects of the 2011 Flood in Thailand on Birth Outcomes and Perceived Social Support. *J. Obstet. Gynecol. Neonatal Nurs.* **2014**, *43*, 435–444.
51. Nabangchang, O.; Allaire, M.; Leangcharoen, P.; Jarungrattanapong, R.; Whittington, D. Economic Costs Incurred by Households in the 2011 Greater Bangkok Flood. *Water Resour. Res.* **2015**, *51*, 58–77.
52. Fernandez, A.; Black, J.; Jones, M.; Wilson, L.; Salvador-Carulla, L.; Astell-Burt, T.; Black, D. Flooding and Mental Health: A Systematic Mapping Review. *PLoS ONE* **2015**, *10*, e0119929.
53. Kittipongvises, S.; Mino, T. Perception and Communication of Flood Risk: Lessons Learned about Thailand's Flood Crisis of 2011. *Appl. Environ. Res.* **2015**, *37*, 57–70.
54. Abuukaz, A.K.; Al-Rawabdeh, A.; Al-Huda, Z.; Dayi, L.; Al-Shboul, D.A.; Hu, Y. Developing an Urban Heat Vulnerability Index Based on Local Climate Zones: A Hybrid Entropy–Random Forest GIS Framework. *Sustain. Cities Soc.* **2026**, *143*, 107376. https://doi.org/10.1016/j.scs.2026.107376.
55. Mremi, A.S.; Kimwaga, R.; Mulungu, D.M.M.; Izdori, F.J. Flash Flood Risk Assessment and Sanitation Infrastructure Vulnerability in Unplanned Urban Areas: A GIS-Based Analysis of the Sinza River Catchment, Dar Es Salaam. *Environ. Sustain. Indic.* **2026**, *30*, 101170. https://doi.org/10.1016/j.indic.2026.101170.
56. Gangrade, S.; Dhariwal, J. A Framework for Designing Urban Heat Vulnerability Assessment Surveys: Insights from a Scoping Review. *Urban Clim.* **2026**, *67*, 102868. https://doi.org/10.1016/j.uclim.2026.102868.
57. Sohn, W.; Xu, Z.; Lu, G.; Kim, J.-H. An Integrated Vulnerability-Resilience Framework for Climate Risk Assessment in Depopulating Urban Landscapes. *Landsc. Urban Plan.* **2026**, *271*, 105620. https://doi.org/10.1016/j.landurbplan.2026.105620.
58. Moccia, A.; Montolío, C.A.; Coch, H. Integrating Building Characteristics and Access to Climate Shelters to Assess Urban Heat Vulnerability. *Sustain. Cities Soc.* **2026**, *143*, 107340. https://doi.org/10.1016/j.scs.2026.107340.
59. Das, A.; Poddar, S.; Mallick, J.; Hang, H.T.; Talukdar, S. Urban Ecological Risk and Social Vulnerability Assessment for Equitable Climate Resilience Planning in Siliguri, India. *Sustain. Cities Soc.* **2026**, 138, 107176. https://doi.org/10.1016/j.scs.2026.107176.
60. Chitwatkulsiri, D.; Miyamoto, H.; Irvine, K.N.; Pilailar, S.; Loc, H.H. Development and Application of a Real-Time Flood Forecasting System (RTFlood System) in a Tropical Urban Area: A Case Study of Ramkhamhaeng Polder, Bangkok, Thailand. *Water* **2022**, *14*, 1641. https://doi.org/10.3390/w14101641.
61. Worawiwat, A.; Chaleeraktrakoon, C.; Sharma, A. Is Increased Flooding in Bangkok a Result of Rising Local Temperatures? *J. Hydrol. X* **2021**, *13*, 100095. https://doi.org/10.1016/j.hydroa.2021.100095.
62. Oswald, J.; Wang, K. A Geodesign Proposal for Bangkok, Thailand. Available online: https://storymaps.arcgis.com/stories/855b9a4491e248579dfc986329856826 (accessed on 16 June 2026).
63. DSD. *Action Plan for Flood Prevention and Mitigation 2026*; Drainage and Sewerage Department BMA: Bangkok, Thailand, 2026; Volume 20.
64. Weng, Q. Remote Sensing of Impervious Surfaces in the Urban Areas: Requirements, Methods, and Trends. *Remote Sens. Environ.* **2012**, *117*, 34–49. https://doi.org/10.1016/j.rse.2011.02.030.
65. BMA. Statistical Profile of BMA 2020. Available online: https://webportal.bangkok.go.th/pipd/page/sub/21303/%E0%B8%AA%E0%B8%96%E0%B8%B4%E0%B8%95%E0%B8%B4%E0%B8%81%E0%B8%A3%E0%B8%B8%E0%B8%87%E0%B9%80%E0%B8%97%E0%B8%9E%E0%B8%A1%E0%B8%AB%E0%B8%B2%E0%B8%99%E0%B8%84%E0%B8%A3-2563 (accessed on 30 May 2026).

66. Zheng, Y.; Xu, S.; Zhou, C.; Wu, Z.; Yang, Y. Spatial Heterogeneity of Driving Factors for Urban Heat Islands and Carbon Emissions: Decoding Priorities, Thresholds, and Synergistic Interactions. *Sustain. Cities Soc.* **2026**, *147*, 107518. https://doi.org/10.1016/j.scs.2026.107518.
67. Zhang, M.; Zhou, D.; Xu, D.; Liu, K.; Gu, Z.; Yang, Y.; Zhang, Q.; Chen, L. How Do Built Environment Factors Influence Urban Heat Islands across Local Climate Zones? Evidence from an Interpretable XGBoost-SHAP Model. *Sustain. Cities Soc.* **2026**, *136*, 107078. https://doi.org/10.1016/j.scs.2025.107078.
68. Chen, Y.; Dong, Q.; Yuan, C.; Zhang, L.; Sun, C. Warming amidst Depopulating: Insights from Surface Urban Heat Island in China's Shrinking Cities. *Habitat Int.* **2026**, *170*, 103758. https://doi.org/10.1016/j.habitatint.2026.103758.
69. Chen, J.; Wang, L.; Ma, L.; Fan, X. Quantifying the Scale Effect of the Relationship between Land Surface Temperature and Landscape Pattern. *Remote Sens.* **2023**, *15*, 2131. https://doi.org/10.3390/rs15082131.
70. Peungnumsai, A.; Miyazaki, H.; Witayangkurn, A.; Kim, S.M. A Grid-Based Spatial Analysis for Detecting Supply–Demand Gaps of Public Transports: A Case Study of the Bangkok Metropolitan Region. *Sustainability* **2020**, *12*, 10382. https://doi.org/10.3390/su122410382.
71. Wang, X.; Chen, B.; Li, X.; Zhang, Y.; Ling, X.; Wang, J.; Li, W.; Wen, W.; Gong, P. Grid-Based Essential Urban Land Use Classification: A Data and Model Driven Mapping Framework in Xiamen City. *Remote Sens.* **2022**, *14*, 6143. https://doi.org/10.3390/rs14236143.
72. Deng, H.; Liu, K.; Feng, J.; Xiong, Y. Tackling the Modifiable Areal Unit Problem: Enhancing Urban Sustainability through Improved Land Surface Temperature and Its Influencing Factors Analysis. *Sustain. Cities Soc.* **2024**, *114*, 105747. https://doi.org/10.1016/j.scs.2024.105747.
73. Andrade, C. Z Scores, Standard Scores, and Composite Test Scores Explained. *Indian J. Psychol. Med.* **2021**, *43*, 555–557. https://doi.org/10.1177/02537176211046525.
74. Ouma, Y.O.; Tateishi, R. Urban Flood Vulnerability and Risk Mapping Using Integrated Multi-Parametric AHP and GIS: Methodological Overview and Case Study Assessment. *Water* **2014**, *6*, 1515–1545. https://doi.org/10.3390/w6061515.
75. Roy, B.; Bari, E. Examining the Relationship between Land Surface Temperature and Landscape Features Using Spectral Indices with Google Earth Engine. *Heliyon* **2022**, *8*, e10668. https://doi.org/10.1016/j.heliyon.2022.e10668.
76. Yuan, F.; Bauer, M.E. Comparison of Impervious Surface Area and Normalized Difference Vegetation Index as Indicators of Surface Urban Heat Island Effects in Landsat Imagery. *Remote Sens. Environ.* **2007**, *106*, 375–386. https://doi.org/10.1016/j.rse.2006.09.003.
77. OECD; European Union; EC-JRC. *Handbook on Constructing Composite Indicators: Methodology and User Guide*; OECD Publishing: Paris, France, 2008. Available online: https://www.oecd.org/en/publications/handbook-on-constructing-composite-indicators-methodology-and-user-guide_9789264043466-en.html (accessed on 31 May 2026).
78. Chitwatkulsiri, D.; Charoenpanuchart, R.; Theepharaksapan, S.; Irvine, K.N. Assessing the Feasibility of Pervious Concrete Blocks for Urban Flood Mitigation in Bangkok Using Hydrological Modeling. *Results Eng.* **2026**, *29*, 108612. https://doi.org/10.1016/j.rineng.2025.108612.
79. Lee, J.; Chung, G.; Park, H.; Park, I. Evaluation of the Structure of Urban Stormwater Pipe Network Using Drainage Density. *Water* **2018**, *10*, 1444.
80. Li, H.; Yan, C.; Zhou, C.; Zhou, L. Building Virtual Drainage Systems Based on Open Road Data and Assessing Urban Flooding Risks. *Water* **2026**, *18*, 341.
81. Tiwari, M.; Shukla, K.; Shukla, S.; Mishra, V.N.; Rawat, K.S.; Singh, S.K.; Pandey, S.; Jamjareegulgarn, P. GIS–AHP-Based Assessment of Urban Waterlogging Susceptibility in Delhi Using Multi-Source Geospatial Data. *Sustain. Resilient Infrastruct.* **2026**, 1–25. https://doi.org/10.1080/23789689.2026.2744500.
82. Goodchild, M.F.; Haining, R.P. GIS and Spatial Data Analysis: Converging Perspectives. *Pap. Reg. Sci.* **2004**, *83*, 363–385. https://doi.org/10.1007/s10110-003-0190-y.
83. Musikhin, I. Spatial Analysis Tool for Urban Environmental Quality Assessment: Leveraging Geoinformatics and GIS. *RIG* **2025**, *34*, 939–957. https://doi.org/10.32604/rig.2025.071168.
84. Ashley, R.M.; Balmforth, D.J.; Saul, A.J.; Blanskby, J.D. Flooding in the Future--Predicting Climate Change, Risks and Responses in Urban Areas. *Water Sci. Technol.* **2005**, *52*, 265–273.
85. Mohamed, A.; Lorestani, N.; Shabani, F. Impact of Urbanization on Land Surface Temperature: A Global Perspective. *Curr. Res. Environ. Sustain.* **2025**, *10*, 100315. https://doi.org/10.1016/j.crsust.2025.100315.
86. Su, M.D.; Lin, M.-C.; Wen, T.H. Spatial Mapping and Environmental Risk Identification. In *Encyclopedia of Environmental Health*; Elsevier: Amsterdam, The Netherlands, 2011; pp. 228–235. https://doi.org/10.1016/B978-0-444-52272-6.00636-X.

87. Wong, D.W. Modifiable Areal Unit Problem. In *International Encyclopedia of Human Geography*; Elsevier: Amsterdam, The Netherlands, 2009; pp. 169–174. https://doi.org/10.1016/B978-008044910-4.00475-2.
88. Cutter, S.L.; Boruff, B.J.; Shirley, W.L. Social Vulnerability to Environmental Hazards. *Soc. Sci. Q.* **2003**, *84*, 242–261. https://doi.org/10.1111/1540-6237.8402002.
89. Ghasemzadeh, B.; Zarabadi, Z.S.S.; Majedi, H.; Behzadfar, M.; Sharifi, A. A Framework for Urban Flood Resilience Assessment with Emphasis on Social, Economic and Institutional Dimensions: A Qualitative Study. *Sustainability* **2021**, *13*, 7852.
90. Balica, S.; Wright, N.G. Reducing the Complexity of the Flood Vulnerability Index. *Environ. Hazards* **2010**, *9*, 321–339. https://doi.org/10.3763/ehaz.2010.0043.
91. Balica, S.F. Development and Application of Flood Vulnerability Indices for Various Spatial Scales. Master's Thesis, UNESCO-IHE Institute for Water Education, Delf, The Netherlands, 2007; p. 9.
92. Koks, E.E.; Jongman, B.; Husby, T.G.; Botzen, W.J.W. Combining Hazard, Exposure and Social Vulnerability to Provide Lessons for Flood Risk Management. *Environ. Sci. Policy* **2015**, *47*, 42–52. https://doi.org/10.1016/j.envsci.2014.10.013.
93. He, C.; Zhou, L.; Ma, W.; Wang, Y. Spatial Assessment of Urban Climate Change Vulnerability during Different Urbanization Phases. *Sustainability* **2019**, *11*, 2406. https://doi.org/10.3390/su11082406.
94. Gomez Vaca, A.N.; Popartan, L.A.; Nuss-Girona, S.; Rodríguez-Roda, I. Spatial Approach for Assessing Vulnerability to Urban Flooding: A Proposal for a Multidimensional Index. *Nat. Hazards* **2025**, *121*, 16799–16825. https://doi.org/10.1007/s11069-025-07451-5.
95. Sun, D.; Mi, X.; Zhang, Z.; Guo, C.; Chenyan, T.; Zhao, S. A Social Media Driven Model for Evaluating Coupled Flood Damage and Resilience at a Fine Scale. *Sci. Rep.* **2026**, *16*, 14451. https://doi.org/10.1038/s41598-026-44294-x.
96. Rui, J.; Gong, W. Social Media-Driven Multi-Scale Flood Sensing: A Systematic Review of Applications from Global Monitoring to Community Resilience. *J. Environ. Manag.* **2026**, *407*, 129895. https://doi.org/10.1016/j.jenvman.2026.129895.
97. Gu, H.; Xiao, J.; Shen, D.; Zhang, C.; Xiao, S.; Niu, Z.; Yu, F. A Combination of Social Media and Satellite Data Improves Flood Monitoring in China. *Commun. Earth Environ.* **2026**, *7*, 411. https://doi.org/10.1038/s43247-026-03403-4.
98. Abdrabo, K.I.; Kantoush, S.A.; Esmaiel, A.; Saber, M.; Sumi, T.; Almamari, M.; Elboshy, B.; Ghoniem, S. An Integrated Indicator-Based Approach for Constructing an Urban Flood Vulnerability Index as an Urban Decision-Making Tool Using the PCA and AHP Techniques: A Case Study of Alexandria, Egypt. *Urban Clim.* **2023**, *48*, 101426. https://doi.org/10.1016/j.uclim.2023.101426.
99. Brown, R.M.; McClelland, N.I.; Deininger, R.A.; Tozer, R.G. A Water Quality Index—Do We Dare? *Water Sew. Works* **1970**, *117*, 339–343.
100. Zhou, W.; Li, Y.; Gou, M.; Wang, B.; Fang, C. Urban Spatial Vulnerability Analysis Based on Urban Systems Using Support Vector Machine. *Sustain. Cities Soc.* **2025**, *123*, 106274. https://doi.org/10.1016/j.scs.2025.106274.
101. Yılmaz, M.; Alemdar, K.D. Mapping and Assessment of Flood Risk Based on Vulnerability and Hazard Factors in Urban Areas through the Integration of Multi-Criteria Techniques and GIS: A Case Study in Yakutiye, Erzurum, Türkiye. *Environ. Earth Sci.* **2025**, *84*, 435. https://doi.org/10.1007/s12665-025-12393-z.
102. OpenStreetMap Contributors. OpenStreetMap. Available online: https://www.openstreetmap.org (accessed on 15 May 2025).
103. Hashimoto, T.; Ito, H.; Yasukawa, A.; Inoguchi, M.; Morishima, A. Collecting and Prioritizing Building Information via Online Microtasks for Tsunami Evacuation Shelter Selection. In *Proceedings of the 23rd International ISCRAM Conference: Building Stronger Futures: Ensuring Public Safety in Times of Crisis, The Hague, The Netherlands, 31 May–3 June 2026*; ISCRAM: Brussels, Belgium, 2026; Volume 23. https://doi.org/10.59297/pkdr3f55.
104. Saguansap, P.; Saguansap, V.; Mruksirisuk, P.; Thanvisitthpon, N.T. Assessment of Urban Heat Island Vulnerability Using Sustainability-Focused Framework: A Case Study of Thailand's Bangkok Metropolis. *Curr. Res. Environ. Sustain.* **2024**, *8*, 100262. https://doi.org/10.1016/j.crsust.2024.100262.
105. Zhang, M.; Liu, Z.; van Dijk, M.P. Measuring Urban Vulnerability to Climate Change Using an Integrated Approach, Assessing Climate Risks in Beijing. *PeerJ* **2019**, *7*, e7018. https://doi.org/10.7717/peerj.7018.
106. Zhang, Y.; Li, X.; Liu, Q. Advancing Urban Resilience: A Multi-Hazard Risk Perspective on Frontier Evolution, Research Hotspots, and Practical Exploration. *Urban Clim.* **2025**, *60*, 102342. https://doi.org/10.1016/j.uclim.2025.102342.
107. Mascheri, G.; Chieffo, N.; Pinto, C.; Lourenço, P.B. Assessing Urban Vulnerability Through a Multi-Hazard Framework with Independent Events Modelling. *Appl. Sci.* **2026**, *16*, 5154. https://doi.org/10.3390/app16105154.
108. Gao, D.; Wang, W.; Yin, J.; Yu, D.; Lu, Y.; Yuan, X.; Li, M.; Yang, Y. Validation of Flood Inundation Modelling Using Multi-Source SAR Imagery. *Water Res.* **2026**, *296*, 125590. https://doi.org/10.1016/j.watres.2026.125590.
109. Antoniou, V. Volunteered Geographic Information, Citizen Science and Machine Learning in the Service of Sustainable Development Goals and the Sendai Framework. *Citiz. Sci. Theory Pract.* **2023**, *8*. https://doi.org/10.5334/cstp.568.

110. Goodchild, M.F. Citizens as Sensors: The World of Volunteered Geography. *GeoJournal* **2007**, *69*, 211–221. https://doi.org/10.1007/s10708-007-9111-y.
111. Choo, W.; Lee, S.; Son, S.; Park, M.; Park, S. A Study on the Implementation of Flood Monitoring and Access Warning System Using CCTV and Image Preprocessing. In *Proceedings of the Construction Applications of Virtual Reality, Volume I*; Noroozinejad Farsangi, E., Rasouli, A.H., Dawood, N., Morrison, G., Eds.; Springer Nature: Singapore, 2025; pp. 167–174.
112. Choi, W.; Kim, S.; Aung, P.P.W.; Lee, C.; Park, S. Real-Time Anticipatory Urban Flood Warning Using CCTV and Page–Hinkley Change Detection. *Dev. Built Environ.* **2026**, *25*, 100866. https://doi.org/10.1016/j.dibe.2026.100866.
113. Zhang, Y.; Jaber, F. An Upgraded GIS-Based Multi-Criteria Decision-Making Approach for Flood Control Prioritization Mapping: Case Study of West Dallas-Fort Worth Metroplex. *Ecol. Inform.* **2026**, *93*, 103573. https://doi.org/10.1016/j.ecoinf.2025.103573.

Disclaimer/Publisher's Note: The statements, opinions and data contained in all publications are solely those of the individual author(s) and contributor(s) and not of MDPI and/or the editor(s). MDPI and/or the editor(s) disclaim responsibility for any injury to people or property resulting from any ideas, methods, instructions or products referred to in the content.